8-17-2020

Modulation Schemes and Connectivity in Wireless Underground Channel

Abdul Salam
Purdue University, salama@purdue.edu

Usman Raza
Purdue University

Chapter 4
Modulation Schemes and Connectivity in Wireless Underground Channel

Abstract In this chapter, a through treatment of the modulation schemes for UG Wireless is presented. The e ects of soil texture and water content on the capacity of multi-carrier modulation in WUC are discussed. The multi-carrier capacity model results are analyzed. Moreover, the underground MIMO design for underground communications is explained thoroughly. An analysis of medium access in wireless underground is done as well. Furthermore, the soil properties are considered for cross-layer communications of UG wireless. The performance analysis of traditional modulation schemes is also considered. The soil moisture based modulation approach is also explored in this chapter. The connectivity and diversity reception approaches are discussed for wireless underground communications. The connectivity and interference models are studied for Ad-Hoc and Hybrid Networks. The topology control mechanisms for maintaining network connectivity and explored for maximizing network capacity under the physical models (e.g., the protocol interference model and physical interference model). Moreover, the underground diversity is examined for 3W-Rake receiver and coherent detection along with experimental evaluation and comprehensive analysis of performance of equalization techniques.

4.1 Introduction

Wireless underground communications are implemented with heterogeneous set of communication devices [87], i.e., various UG sensor nodes for sensing and di erent AG nodes for supporting and maintaining infrastructure [33, 41]. In WUC communication range depends on the locations of nodes with respect to the ground surface. Hence, deployment depth should also be considered for deployment analysis in WUSNs [38, 39]. In the following section, we present an in-depth analysis of the underground modulation schemes, deployment, and connectivity.

4.2 Multi-Carrier Modulation: Subcarriers in UG Channel

High data rate is one of the important requirement of IOUT. Data rate is highly dependent on IOUT communication channel , however, IOUT channel characteristics are not modeled. Therefore, extensive experimentation is required to characterize IOUT wireless channel. Soil properties (moisture, and type) and antenna properties (burial depth and distance) impacts capacity of communication channel. Therefore, there is a need to develop a theoretical model to estimate the channel capacity of IOUT channel considering all these factors [47, 51].

4.2.1 Capacity Model

The channel capacity depends upon the bandwidth and change in transfer function with the change in bandwidth [50]. Therefore, two properties of UG channel are considered for channel capacity model: 1) bandwidth of the sender and receiver antenna, and 2) channel transfer function. Bandwidth is determined from return loss of an antenna. Return loss occurs due to impedance mismatch which and can be calculated as:

$$RL_{\,\mathrm{dB}} = 20\log_{10}\left|\frac{Z_s + Z_a}{Z_s - Z_a}\right|, \tag{4.1}$$

where Z_s represents the transmission line and Z_a represent impedance of antenna.

Fig. 4.2(a) plots return loss of antenna at zero (0) soil matric potential. Bandwidth is calculated using a threshold value δ for antenna return loss. Generally, a value of $-10\,\mathrm{dB}$ is used for δ in existing literature [4, 27]. It is assumed that the receiver and sender will have same return loss. The reason for this assumption is that short distance and spatial homogeneity of soil reduces the probability of di erence in resonant frequency and return loss of antennas at sender and receiver. Bandwidth of an antenna is maximum at its resonant frequency, therefore, second assumption is that the system is operating at resonant frequency to maximize the bandwidth [10, 30]. Bandwidth of an underground system with the antenna operating at resonant frequency is given as:

$$B_s = \begin{cases} 0 & \text{if } -R(f) > \delta, \\ 2(f - f_m) & \text{if } -R(f) \leq \delta \; and \; f < f_r, \\ 2(f_M - f) & \text{if } -R(f) \leq \delta \; and \; f \geq f_r, \end{cases} \tag{4.2}$$

where f_r is the resonant frequency, f_m is lowest and f_M is the highest frequency at which $R(f) \leq \delta$.

The total number of sub-carriers are calculated in a multi-carrier modulation. Here, a total number of sub-carriers are defined as the least number required to prevent

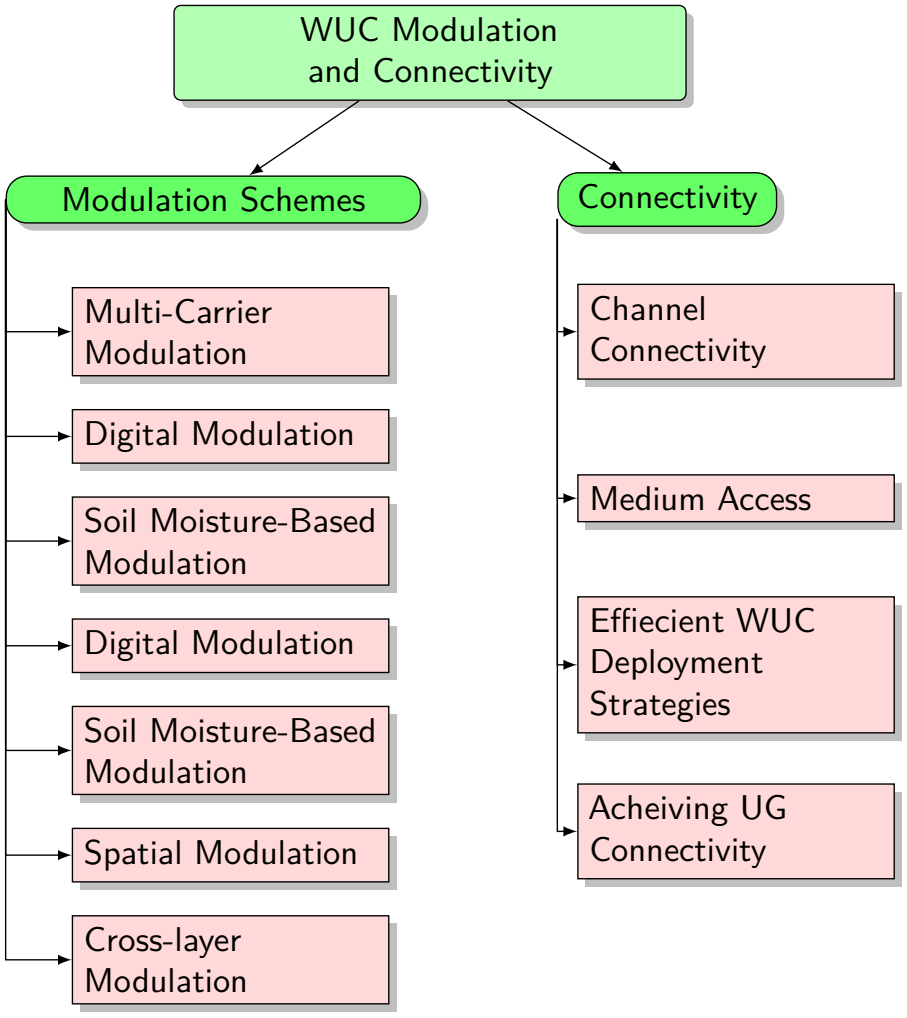

Fig. 4.1: Organization of the Chapter

inter-symbol interference (ISI) due to on B_s (system bandwidth). The total number of sub-carriers are given as:

$$N_c = \left\lceil \frac{B_s}{B_{cb}} \right\rceil. \tag{4.3}$$

where B_{cb} is the channel coherence bandwidth.

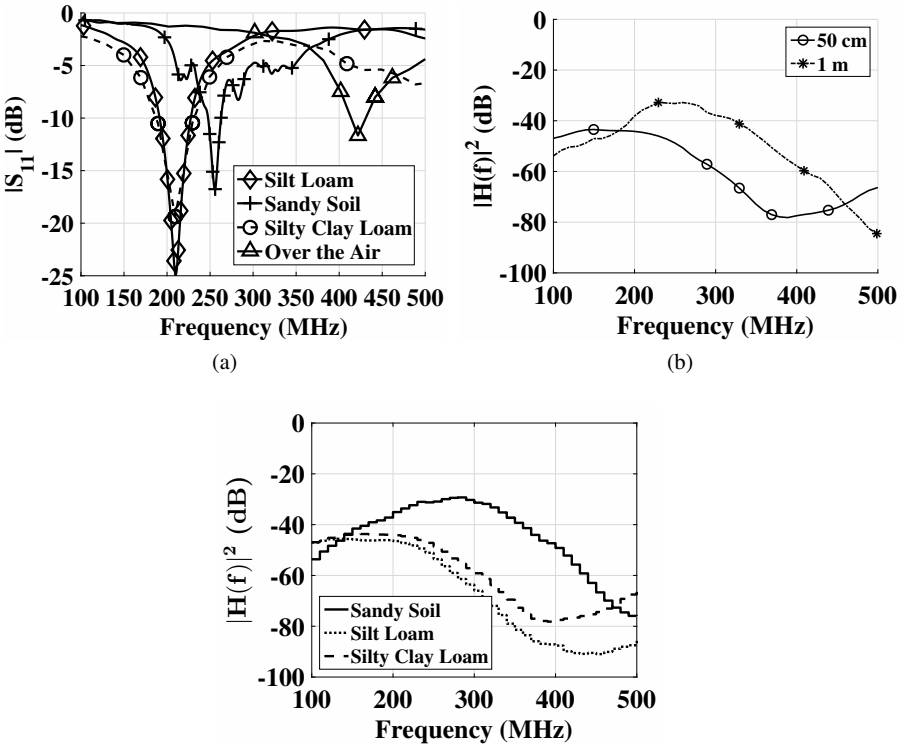

Fig. 4.2: (a) Antenna Return Loss at 0 CB [47], (b) Channel transfer function [47], (c) Approximating Channel Transfer Function at the distance and depth of $50\,\mathrm{cm}$ and $20\,\mathrm{cm}$, respectively [47]

The spectral efficiency of m-ary quadrature amplitude modulation (MQAM) is high. Therefore, MAQM is considered as a modulation method for each sub-carrier [27, 39]. Total bit rate of the UG channel is calculated as:

$$R_{ug} = \sum_{i=1}^{N_c} r_i B_{cb}, \tag{4.4}$$

where N_c is the total number of sub-carriers in a multi-carrier transmission system, B_{cb} is the bandwidth of an individual sub-carrier, and r_i is the bits per symbol for each carrier.

At high signal-to-noise ratio (SNR), the symbol-error probability, P_{sc}, for each of the i-th carrier is calculated as:

$$P_{sc_i} = K_{ri} Q\left(\sqrt{\frac{3En}{(M_i - 1)N_0}}\right), \tag{4.5}$$

The value of a constant K_{ri} is dependent upon the total bits per symbol. Its value lies in the range of $2 \leq K_{ri} < 4$.

$$\sum_{i=1}^{N_c} \gamma_i \cdot P = P, \quad \gamma_i > 0. \tag{4.6}$$

Power allocation among sub-carriers can be optimized based on target probability of symbol error for each sub-carrier, $P_{sc}^{*} > P_{sc_i}, \forall i$, and a constant power constraint P. It also maximizes the bit rater of UG channel, R_{ug}.

Fig. 4.2(b) plots the empirical channel transfer function for sandy soil at a distance of $50\,\mathrm{cm}$ and $1\,\mathrm{m}$. For the individual lower bandwidths, B_{cb}, staircase function gives close approximation of channel transfer function $\mid H(f) \mid^2$. Therefore, the transfer function is approximated using a staircase function, $\mid \hat{H(f)} \mid^2$. Fig. 4.2(c) shows the staircase approximation of channel transfer function in sandy soil at $20\,\mathrm{cm}$ depth and $50\,\mathrm{cm}$ T-R distance. The total bit rate of UG channel is given as summation of all sub-carriers [22]:

$$R_{ug} = \sum_{i=1}^{N_c} B_{cb} log_2 \left\{ 1 + \frac{3\gamma_i P}{\frac{(N_0 B_{cb}) \mid H_i(f) \mid^2}{\left[Q^{-1}\left\{\frac{P_{sc}^{*}}{K_{ri}}\right\}\right]^2}} \right\}, \tag{4.7}$$

where N_c is from equation 4.3, P is transmit power constraint and γ's are given such that:

R_{ug} is maximized by optimized power distribution among sub-carriers. This optimization problem [32, 33, 48, 85] is solved similar to as water filling problem of [8, 10, 46] was solved. Langrangian multiplier is used to obtain the optimized power allocation, γ_i^{*}, leading to water filling allocation as [10, 33]:

$$\gamma_i^{*} = \begin{cases} \lambda - \frac{1}{K_0 |H(f)_i|^2)} & \text{if } \gamma_i > 0, \\ 0 & \text{otherwise,} \end{cases} \tag{4.8}$$

where $\sum_{i=1}^{N_c} \gamma_i^{*} = 1$, and $K_0 = 3P/(N_0/[Q^{-1}[.]]^2)$. An updated maximum bit rate, R_{ug}^{max} is calculated by jointly solving equation 4.6 and equation 4.8 [22, 28]. R_{ug}^{max} is given as:

$$R_{ug}^{max} = \sum_{i=1}^{N_c} B_{cb} \cdot log_2 \left\{ \lambda K_0 \mid H_i(f) \mid^2 \right\}, \tag{4.9}$$

This rate is a high-SNR optimal because it is for the cases having high-SNR. Another sub-optimal solutions for an equal power allocation to sub-carriers has capacity close to that of an optimal solution [9, 26, 32, 35]. R_{ug} for equal power allocation is calculated as:

$$R_{ug}^{eq} = \sum_{i=1}^{N_c} B_{cb} log_2 \left\{ 1 + \frac{\frac{3P/N_c}{(N_0 B_{cb}) \mid H_i(f) \mid^2}}{\left[Q^{-1} \left\{ \frac{P_{sc}^*}{K_{ri}} \right\} \right]^2} \right\}, \tag{4.10}$$

4.2.2 Results and Discussion

E ect of Soil Texture

Figs.4.3 plots the multi-carrier capacity of UG channel. Three di erent types of soil (silty loam, silty clay loam and sandy) are used for the experiments at the distances of $50\,\mathrm{cm}$ (Fig. 4.3(a)) and $1\,\mathrm{m}$ (Fig. 4.3(b)). The e ect of soil type was measured on capacity and system bandwidth. The system bandwidth was calculated as $20\,\mathrm{MHz}$. Sandy soil had the highest capacity at both distances of $50\,\mathrm{cm}$ ($30\,\%$ higher) and $1\,\mathrm{cm}$ ($39\,\%$ higher). This is because attenuation of EM waves in soil is dependent upon the water holding capacity of a soil and sandy soil has lowest water holding capacity as compared to silty loam and silty clay loam. Therefore, soil with lower clay content (sandy soil) experiences minimum attenuation. Channel capacity decreases for each type with increase in distance. For sandy soil it went from $233\,\mathrm{Mbps}$ to $180\,\mathrm{Mbps}$, $195\,\mathrm{Mbps}$ to $137\,\mathrm{Mbps}$ for silty clay loam soil, and $178\,\mathrm{Mbps}$ to $129\,\mathrm{Mbps}$ for silty loam soil. This is because of EM signals attenuates with the increase in distance [29].

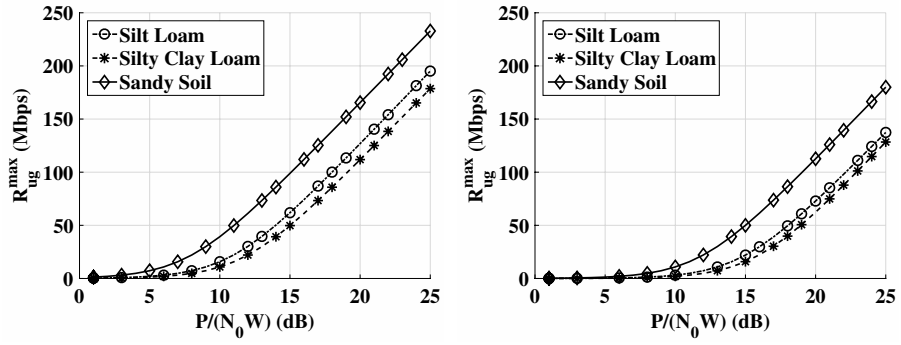

(a) (b)

Fig. 4.3: Channel Capacity for $200\,\mathrm{MHz}$ bandwidth and $20\,\mathrm{cm}$ depth, at distance of [47]: (a) $50\,\mathrm{cm}$, total number of sub-carriers are 25 (sandy), 25 (silty clay loam), and 24 (silt loam), (b) $1\,\mathrm{cm}$, total number of sub-carriers are 27 (sandy), 21 (silty clay loam), and 25 (silt loam)

4.2.2.1 E ect of Soil Moisture

Figs. 4.4 plots the e ect of soil moisture on various parameters of multi-carrier capacity of UG channel. Fig. 4.4(a) shows antenna bandwidth against soil moisture in a silt loam soil. Antenna bandwidth increases upto $80\,\%$ (i.e., from $20\,\mathrm{MHz}$ to $36\,\mathrm{MHz}$) with the decrease in soil moisture. Fig. 4.4(b) shows the coherence bandwidth & number of sub-carriers plotted against soil moisture in a silt loam soil. The coherence bandwidth decreases upto $69\,\%$ (i.e., from $55\,\mathrm{kHz}$ to $17\,\mathrm{kHz}$) and number of sub-carriers increased by $175\,\%$ (i.e., from 20 to 55) as the soil moisture decreases. The impact on sub-carrier can be minimized by adjusting sub-carrier bandwidth [24].

Figs. 4.4(c) and 4.4(d) shows the maximum bit rate from equation 4.9, with soil moisture in silt loam and sandy soil, respectively. For both soils, with increasing value of (P/N_0W), the bit rate increases with decrease in soil moisture, e.g., for

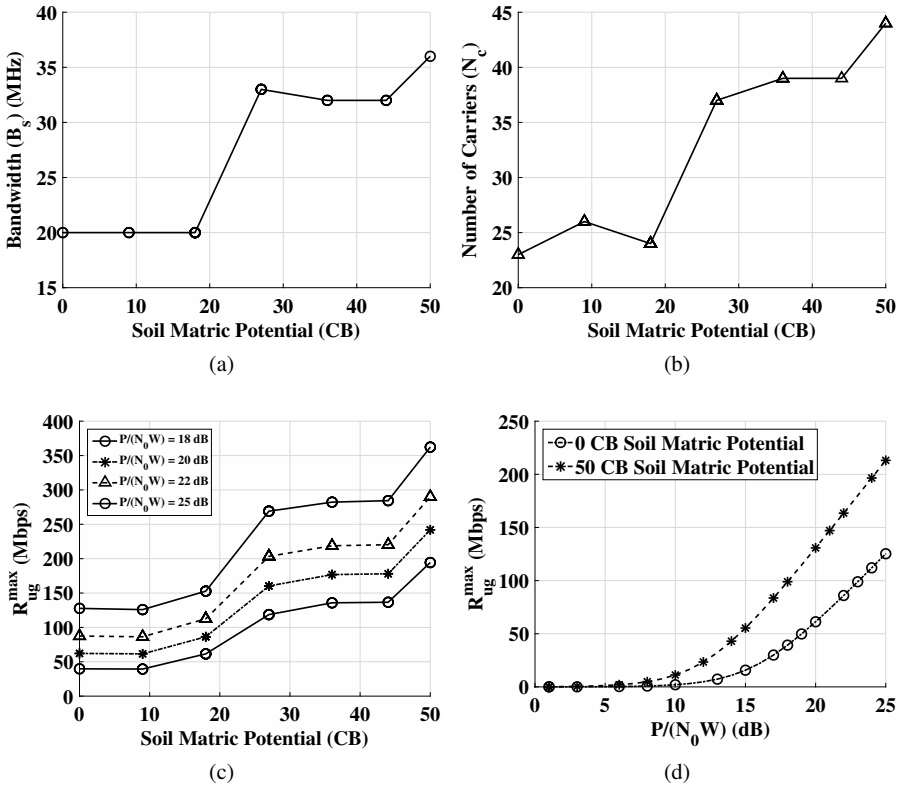

Fig. 4.4: Soil moisture impact in silt loam soil [47]: (a) System bandwidth, (b) Number of sub-carriers, (c) Data rate, (d) Channel capacity depth and distance of $20\,\mathrm{cm}$ and $50\,\mathrm{cm}$, respectively, in sandy soil

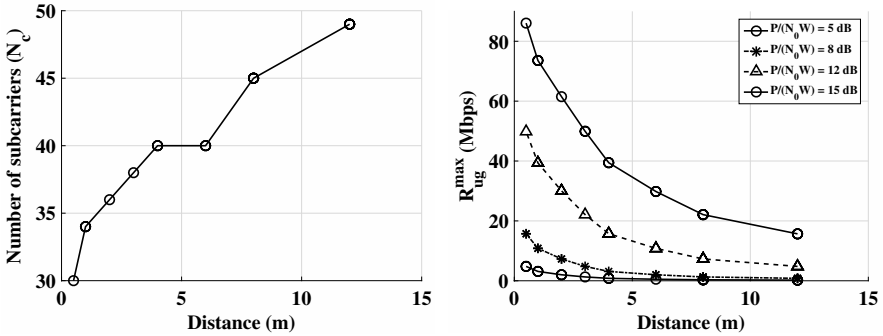

(a) (b)

Fig. 4.5: E ect of distance on [47]: (a) Underground channel capacity , (b) Number of sub-carriers (N_c)

(P/N_0W) = 18 dB, rate increases from 39 Mbps to 194 Mbps, and for and (P/N_0W) = 25 dB it goes from 127 Mbps to 362 Mbps. Similarly for sandy soil, data rate is increased from 126 Mbps to 213 Mbps. EM waves are absorbed by soil water content causing more attenuation. Change in soil moisture changes soil permittivity resulting in fluctuating wavelength which further attenuates the signal. Therefore, decrease in soil moisture lowers signal attenuation, increasing data rate[32].

4.2.2.2 E ect of Distance

Experiments were conducted in an outdoor testbed to study the e ect of distance on the channel capacity. Silty clay loam soil and burial depth of 20 cm are used for experiment. Fig. 4.5(b) shows the number of sub-carriers against distance. It shows that for 20 MHz antenna bandwidth, the coherence bandwidth decreases from 678 kHz to 411 kHz with decrease in distance. This is because RMS varies with change in distance. Fig. 4.5(b) plots T-R distance with channel capacity [41, 44]. It can be seen that a bit rate of 80 Mbps can be achieved at distance up to 12 m. Underground communication is carried out by three component waves: direct, reflected and lateral. As the distance is increased, direct and reflected component fades and the only significant component of the received signal is lateral wave. As the distance is increased further, lateral waves also attenuates, hence, decreasing the data rate.

4.3 Digital Modulation: Wireless UG Receiver Design Based on Diversity

The delay spread of underground channel has adverse e ect on the performance of the channel. It results in frequency selective fading [28, 147]. Frequency selective

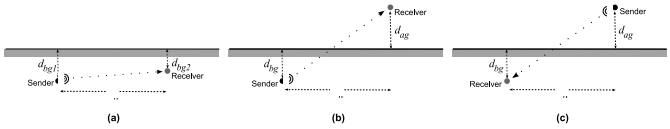

Fig. 4.6: Di erent communication links of WUSNs [57]

fading limits the data rate of the channel and induces an irreducible bit error rates (BER). Therefore, impact of delay spread and resulting frequency selective fading on UG channel is an important issue to investigate [26, 53, 62, 147]. An ideal UG channel must dynamically adapt to soil parameters while achieving high data rate and low BER. To that end channel capacity has already been investigate in [10, 33, 35], however, impact of digital modulation techniques on UG channels is still not investigated. Therefore, this section explain these e ects using the impulse response of UG channel.

4.3.1 Diversity Model

This section develops a model which uses channel impulse response to analyze the impact of RMS delay on conventional modulation techniques, i.e., pulse-amplitude modulation (PAM), di erential phase shift keying (DPSK), quadrature phase shift keying (QPSK), Gaussian minimum-shift keying (GMSK), and m-ary quadrature amplitude modulation (MQAM). The aim is to optimize the IOUT design parameters, i.e., modulation techniques and BER.

The EM-based communication in IOUT consist of three components (see Fig. 4.6: direct, reflected and lateral, out of which lateral wave is the strongest. The impulse response of UG channel is expressed as sum of all these components [41, 147]:

$$h_{ug}(t) = \sum_{l=0}^{L-1} \alpha_l \delta(t-\tau_l) + \sum_{d=0}^{D-1} \alpha_d \delta(t-\tau_d) + \sum_{r=0}^{R-1} \alpha_r \delta(t-\tau_r), \qquad (4.11)$$

where L, D, and R are number of multiple paths; α_l, α_d, and α_r, are complex gains; and τ_l, τ_d, τ_r are delays for lateral, direct and reflected wave component. These measurements were taken in indoor and outdoor testbeds. The experiment setup details are given in [37, 40, 147].

The output waveform of the received signal is given by the convolution of the baseband input to UG channel, $u(t)$ and channel impulse response, h_{ug} as follow:

$$z(t) = u(t) * h_{ug}, \qquad (4.12)$$

Using equation 4.11, the waveform can expressed as follow:

$$z(t) = \sum_{l=0}^{L-1} \alpha_l u(t-\tau_l) + \sum_{d=0}^{D-1} \alpha_d u(t-\tau_d) + \sum_{r=0}^{R-1} \alpha_r u(t-\tau_r), \tag{4.13}$$

The delay spread of the UG channel, τ_d is normalized using sample period T and RMS delay spread τ_{rms} as follow:

$$\tau_d = \frac{\tau_{rms}}{T}, \tag{4.14}$$

Bandwidth is calculated as $B = 1/T$. The input signal, $u(t)$ is convolved with signaling waveform $u(t)$ for all modulation schemes. For signaling, raised cosine pulses and rectangular waveform were used. The advantage of raised cosine waveform is that raised cosine filter reduces the ISI and can be realized through raised cosine spectrum with β as a roll-o factor. BER performance is calculated at receiver [38, 42].

The impulse response h_{ug} has been calculated from PDPs measured using di erent soil parameters (moisture level, depths and distances).

UG 3W-Rake Receiver The purpose of designing UG 3W-Rake Receiver is to minimize the multipath fading in the system, however, it is done without considering spatial diversity. The approach is based on RAKE [29, 43] and resolve the fading of three components of waves, namely, direct, reflected and lateral. It exploits the high diversity of all three components. UG 3W-RAKE has a branch for each component which correlates the corresponding component of the received signal, thus, separating all components.

Signal-to-Noise ratio of an underground received signal is random. This is because of multipath fading happening in underground. Therefore, error probability of Additive White Gaussian Noise (AWGN) is averaged over the probability density function (pdf) of the SNR$_{\gamma b}$. Average BER probability, $P_b(\bar{\gamma}b)$

$$P_b(\bar{\gamma}) = \int_0^{\infty} P_{e|\gamma_b} p(\gamma_b) d_{\gamma_b} \tag{4.15}$$

where $\bar{\gamma}_b$ is average SNR/bit, $p(\gamma_b)$ is pdf of SNR,and $P_{e|\gamma_b}$ is conditional AWGN error probability. There is no close form solution available for the pdf of γ_b, therefore, $p(\gamma_b)$ is measured from UG channel response experiments [147]. It is done, for each measured response, by averaging $P_{e|\gamma_b}$ over instantaneous SNR. As UG 3W-Rake is for the processing of multi-paths in all three components of wave, the SNR per received bit γ_b is calculated as:

$$\gamma_b = \sum_{l=0}^{L-1} \gamma_l + \sum_{d=0}^{D-1} \gamma_d + \sum_{r=0}^{R-1} \gamma_r, \tag{4.16}$$

Equation 4.16 can be rewritten as:

$$\gamma_b = \frac{E_b}{N_0} \left[\sum_{l=0}^{L-1} \mid \gamma_l \mid^2 + \sum_{d=0}^{D-1} \mid \gamma_d \mid^2 + \sum_{r=0}^{R-1} \mid \gamma_r \mid^2 \right], \tag{4.17}$$

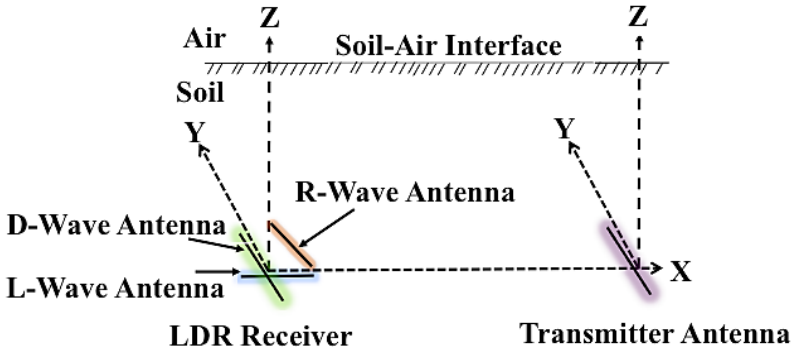

Fig. 4.7: The underground antenna positions [64]

where $\frac{E_b}{N_0}$ is the ratio of energy per bit to noise power spectral density (PSD) and calculated as:

$$\frac{E_b}{N_0} = \frac{P_t T}{N_0 PL} \tag{4.18}$$

where P_t is the power transmitted, N_0 is the noise density, T is the sample period and PL is path loss.

This process is used to approximate a discrete $p(\gamma)$. After the calculation of $p(\gamma)$, average bit rate probability, $P_b(\bar{\gamma})$, is calculated using equation 4.15.

LDR Receiver Design This section discusses the development procedure of a novel LDR reception technique.considering di erent parameters of UG communication such as delay spreads, angular angle and travel path. It shows significant increase in performance as compared to existing techniques. The key characteristics of the technique are: elimination of multi-path fading and elimination of inter-symbol-interference between three components (lateral, direct and reflected) of waves.

LDR Antenna Orientation: Both, transmitter and receiver, are buried in considered IOUT system. Transmitter is equipped with single antenna and receiver is equipped with three antennas, one for each wave component [34]. For diversity reception of the UG channel, LDR antenna orientation is shown in Fig. 4.7. To receive direct wave (D-wave), corresponding receiving antenna is aligned at $90°$ from x-axis. To receive reflected wave (R-wave) , corresponding receiving antenna is aligned at the connecting line of x-axis and z-axis with center at $45°$ from x-axis. To receive Lateral wave (L-wave), corresponding receiving antenna is aligned at $0°$ from x-axis. Same depth is assumed for transmitter and receiver antenna along the x-axis to avoid variations in axis of the receiver [36].

LDR System Model: For the antenna orientation in Fig. 4.7, received signal is calculated as:

$$z = h_{ug} u + n \tag{4.19}$$

where z is a 3×1 vector for received output, u is the transmitter's data symbol, h_{ug} is the vector for channel impulse response for wave components (L-, D-, R-wave channel response) and n is the 3×1 vector for noise. Channel response of each wave component can be separated as $h_d$for direct, $h_r$for reflected, $and h_l$for lateral. Instantaneous SNR for each receiving antenna is defined as:

$$\gamma_i = \frac{E_b \mid h_i \mid^2}{N_0}, \tag{4.20}$$

where $i = L, D,$ and$R$ components.

Optimum Maximum Ratio Combining (MRC-LDR): SNR can be determined by using maximum ratio combining (MRC) [29, 39, 44]. This SNR is increase three times from the SNR of a single antenna matched filter UG receiver:

$$\gamma = \sum_{i=1}^{3} w_i \frac{E_b \mid h_i \mid^2}{N_0}, \tag{4.21}$$

where w_i is the combining weight. Although, MRC-LDR achieves the maximum gain, however, interference due to reflected component is still present. The suppression of this interference is discussed in the next section.

Adaptive Combining (AC-LDR): Among the three components of the signal wave, one of either D-wave or L-wave is dominant at receiver end [51]. This dominance rely on the proximity of LDR receiver. AC-LDR use this fact to, dynamically, switch and adapt strongest of the two components (L and D). R-component is not considered because of being the weakest among all and may cause the performance to degrade as:

$$\gamma = \begin{cases} \frac{E_b|h_L|^2}{N_0}, & \text{if } \mid h_L \mid^2 > \mid h_D \mid^2, \\ \frac{E_b|h_D|^2}{N_0}, & \text{otherwise.} \end{cases} \tag{4.22}$$

AC-LDR di ers from MRC-LDR in that it removes interference while achieving channel gain. For both LDR approaches, the average BER, $P_b(\bar{\gamma_b})$, is calculated as [29, 51]:

$$P_b(\bar{\gamma}) = \int_0^\infty P_{e|\gamma_b} p(\gamma_b)\, d_{\gamma_b}, \tag{4.23}$$

4.3.2 Performance Analysis

Power delay profile of multi-path UG channel is dependent upon the depth and moisture of the soil, and depths and distance of the UG antennas (transmitting and receiving). The UG channel is simulated by with the range of 0.4-0.002 for τ_d.

1. **Coherent Detection**: This section analyze the performance of modulation techniques, namely, QAM, PSK, PAM, and MSK. The parameter used for the

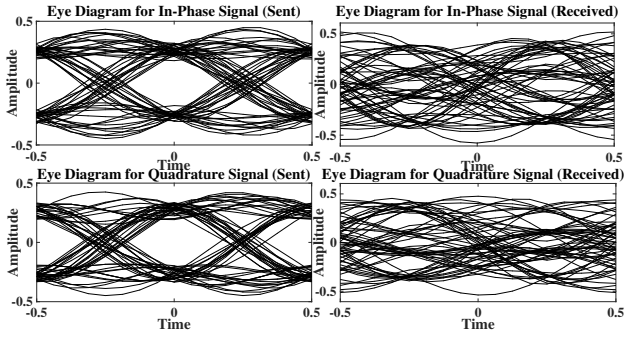

(a)

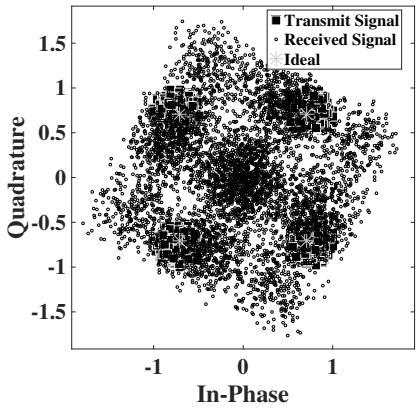

(b)

(c)

Fig. 4.8: (a) QPSK eye patterns, (b) QPSK constellation diagram, and (c) Experiment setup for estimating BER [64]

experiments are: soil type is silty clay loam, soil moisture is 0 CB and τ_{rms} is 25ns, distance between transmitter and receiver antenna is 50cm, and burial depth of antenna is 20cm. Very high error rates ($< 10^{-1}$) were observed for all modulation techniques. This is because of the e ect of multipath fading in UG channel. The coherent modulation technique require the knowledge of exact state of UG channel, however, higher delay spread makes it difficult ot track reference symbol for the channel. Moreover, it was observed that error rate is independent of the sample time because it does not change for the τ_d range of 0.002-0.4. Fig. 4.8(a) and 4.8(b) shows the plot of constellation and eye diagram, respectively, for QPSK modulation. It can be seen from Fig. 4.8(a), that inter-symbol interference and large delay spread between wave components causes severe detonation and complete eye closure which consequently result in high error rate. Hence, digital modulation in UG channel highly a ected by multipath fading and does not improve by increasing the power rate. The empirical validation of results is shown in coming sections [24, 46].

2. **Experimental Evaluation:** Experimental setup for BER performance analysis under UG channel is shown in Fig. 4.8(c). It consist of a: GNU Radio [30, 30], Ettus N210 USRPs [31, 49], burial depth is 20cm, distance is 50cm and soil is silty clay loam soil, moisture level is 50Cb, $\tau_{rms} = 25.67ns$ [41, 147], transmit power is 10dBm, range for operational frequency is 100 - 300 MHz and normalized delay spread, τ_d range from 0.005-0.43. The Amplitude-shift keying (ASK) modulation technique is used for the experiment.
   Experiments were conducted on software defined radio (SDR). The results shows very high bit rate further proving the vulnerability of UG channel to multipath fading and delay spread. In over-the-air (OTA), this can be minimized by using adaptive equalization.
3. **Di erential Detection:** Di erential quadrature phase shift keying (DQPSK) and di erential binary phase shift keying (DBPSK) were used with $\tau_{rms} = 25ns$ to analyze the performance of UG channel. Fig. 4.9(a) compares the BER performance of DQPSK and DBPSK. It can be seen that with τ_d values less than 0.1, error rate reduces by 10^-3 which is significant improvement over the error rate of 10^-1 for coherent modulation schemes.The error rate increases with increase in value of τ_d, however, di erential schemes are relatively performing better [29, 52].
4. **3W-Rake Performance in UG Channel:** This section analyze the performance of 3W-Rake receiver. In order to achieve the target BER thresholds, SNR values are analyzed under di erent modulation schemes. Di erent combination of soil types, soil moisture levels, burial depth and distances between transmitter and receiver were considered for the experiments. Fig. 4.9(b) plots the BER along with changing depth in silt loam soil at distance of 50cm and 1m. It can be seen that BER increases with the increase in burial depth, however, the increase is relatively greater when the distance between the antennas is greater. Fig. 4.9(c) plots the BER along with distances less than 1m in silty clay loam soil. It can be observed that BER increases with the increase in distances because propagation loss of all three components increases with the distance which causes attenuation

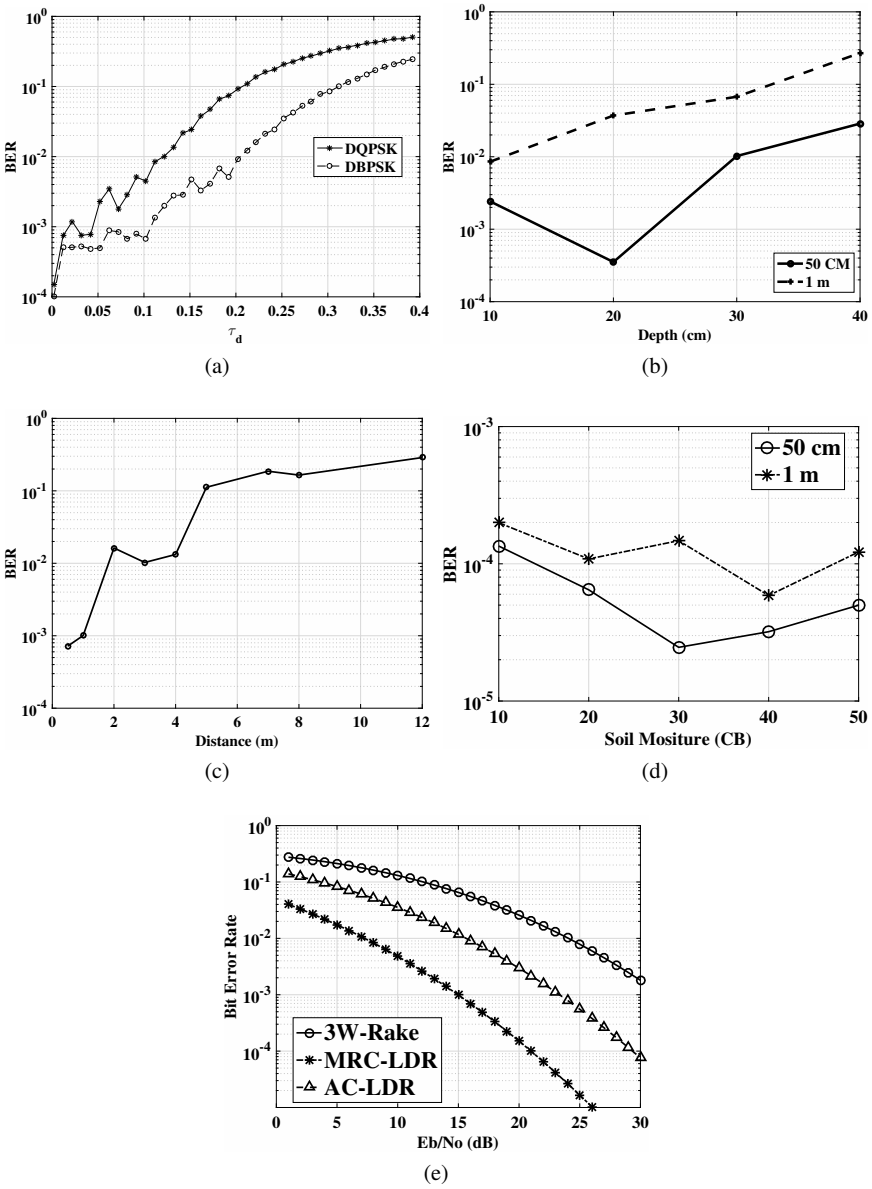

Fig. 4.9: Bit Error rate [64]: (a) using di erent modulation techniques, (b) with varying depths in silt loam soil, (c) with varying distance in silty clay loam soil, (d) with varying soil moisture at two distance in silt loam soil, (e) comparison BER for AC-LDR, 3W-Rake, and MRC-LDR

leading to increase in BER. Similarly, Fig. 4.9(d) plots the BER along with soil moisture range from 0-50 CB at teh distances of 50cm and 1m in silt loam soil. The BER trend is similar for both distances values. It first decreases for initial values of soil moisture and start increasing afterwards. This because of water repellency due to soil texture slowing down the water infiltration at high soil moisture levels [25, 50, 52].

5. **LDR Performance Analysis:** Fig. 4.9(e) compares the performance of 3W-Rake with MRC-LDR and AC-LDR.It can be observed that both LDRs are performing better than 3W-Rake. There is significant improvement for SNR > 13dB. It is because LDR uses separate antenna for each wave component whereas 3W-Rake degrades due to bottleneck while correlating the components.
6. **LDR Implementation:** AC-LDR uses zero-forcing (ZF) precoding for it implementation. ZF precoding performs inversion of channel matrix for the removal of unwanted components. Optimum MRC combining can be implemented using extra digital signal processing (DSP) hardware and it can used as benchmark to analyses the theoretical performance of UG channel. However, LDR is considered more suitable to fulfill the high data rate and long-range of next generation IOUT systems [72].

4.4 Soil Moisture-Based Modulation

In UG communications soil moisture information can be used to design a unique soil moisture-based modulation scheme. The core idea is based on selecting a channel state using the propagation environment in the vicinity of transmit antenna(s), which in turn will change with soil moisture changes. This can be viewed as creating a multitude of channel states, each corresponding to a di erent transmission path, where the transmitter can select any of the channel states in each transmission.

In UG communication, these states are inherently available due to soil moisture changes. This approach enables transmitter to use the information to be transmitted as an index to select a particular channel state. Soil moisture modulation uses channel state variations to embed information in transmission media. It is di erent from conventional wireless communications where data is embedded into a radio frequency prior to transmission.

Media based modulation (MBM) is a similar technique used in conventional wireless systems. It randomize a wireless channel by perturbing the propagation environment in the vicinity of transmit antennas resulting in change of overall transmission path [23, 73]. In contrast to MBM, di erent channel states are inherently available in UG communication due to the dependence of channel on soil moisture.

Soil moisture-based modulation will have M channel states created due to soil moisture variations. A total of $\log_2$(M) bits can be transmitted by selecting any one of these states for transmission. In other words, the UG channel state depends on soil moisture. By selecting the most suitable channel state based on soil moisture, the transmitter not only maximizes the probability of communication success but

also transmits the soil moisture information without incurring any additional cost. Consequently, the soil moisture based modulation scheme allow *resource-free* transmission of soil moisture data. Each channel state and gain will be di erent based on the soil moisture variations, therefore, each state will have its own channel gain which is likely to follow a complex Gaussian distribution.

The strategy investigates practical methods to independently identify the transmission path for each soil moisture state. To convey a particular selection to the receiver, transmitter will then send a signal through the selected channel state.

4.5 Spatial Modulation: Subsurface MIMO

Underground communication is challenging because of impact of soil texture and water content. Range and energy of UG communication can be improved by using phased-array antenna in UG radio wave propagation [25, 54]. The antenna array is used to direct the wave power via Zenneck waves. This section explains the design of UG phased-array of antennas for digital agriculture and develops the underground (UG) multiple-input multiple-output(MIMO) using transmit and receive beamforming in IOUT communication systems.

Underground nodes communicate with other UG nodes via UG2UG link and with aboveground (AG) nodes via UG2AG link. Fig. 4.10 shows the overview of UG MIMO communication system. An aboveground node can be a fixed or mobile sink. A mobile AG sink is attached to some moving infrastructure, e.g., tractors. Soil-air interface has an impact on wave propagation to receiver nodes. For example, it is refracted in AG communication and for UG communication lateral wave are used. Fig. 4.10 shows the beam patterns for UG and AG communication. In Fig. 4.10(b), the UG propagation is e ected due to soil-air interface a ect, i.e., reflected and refracted EM waves. These EM waves e ect the beam pattern which is being propagated towards AG node.

The main purpose of transmit beamforming [49, 63] is to focus energy towards desired direction. The wave can reach receiver from any of three available paths [37, 147] in UG soil medium. When UG receiver is getting the data only from the desired path, UG MIMO channel act as a three-path interference channel, i.e., direct, reflected and lateral. Therefore, capacity of MIMO channel and freedom degree is required to be carefully modeled.

There are three components of EM wave propagating in the soil, i.e., direct, lateral and reflected. UG receiver is required to cancel interference from all these components. The UG MIMO focuses on arrival of the minimum interference signal at the receiver end. It does so by removing the undesired interference that may arise due to undesired components via receive beamforming. An underground MIMO technique is developed using the transmit and receive beamforming which is aware of the UG environment. Accordingly, experiments are performed to test UG MIMO techniques [50, 71].

4.5.1 UG MIMO System Models

Some assumptions made for designing MIMO system are: (1) transmitter and receiver has multiple transmit and receiving antennas, respectively, along with the beamforming capabilities and, (2) transmitter antenna has ability to steer beam and receiving antenna can receive all three component of wave from soil. Receiver has ability to select and switch path using a selection method depending upon the strength of received path at the receiver. It is also assumed that power is equally allocated to all UG MIMO transmitters. Total power constraint is assumed to analyze the capacity of the system. Next, zero-forcing (ZF) UG MIMO transceiver technique is explained as below [36, 55, 72].

Contrary to over-the-air (OTA) MIMO methods, information about receiver channel state is not necessary for ZF UG MIMO transceiver technique. It improves the received signal strength by removing the interference between the components. **TR** is the channel between the transmitter and receiver represented as a complex number. The size of the channel is given as $N_t \times N_r$, where N_t is the number of transmitter antenna and N_r is the number of receiving antenna. A total of k spatial underground components are di erentiated using $w_1, \ldots, w_k$. Each w is associated with a component. Interference between the component is denoted by $N_t \times N_r$ matrix I_k. With equal power constraint, signal at the receiver is given as [7, 20]:

$$y_k = w_k^* TRf_k x_k + w_k^* I_k f_i x_i + w_k^* n_k \tag{4.24}$$

where x_k is the transmitted signal of the UG component k, n_k is additive white Gaussian noise (AWGN) vector, and w_k and f_k represents the transmit and receive beamforming vectors.

Next, capacity maximization expression is evaluated for cases having low SNR values. From equation 4.24, SINR at receiver for k_{th} component is given as:

$$SINR_k = \frac{w_k f_k f_k * TRTR^* w_k^*}{w_k^*(I_k I_k * f_i f_i^*) w_k^*} \tag{4.25}$$

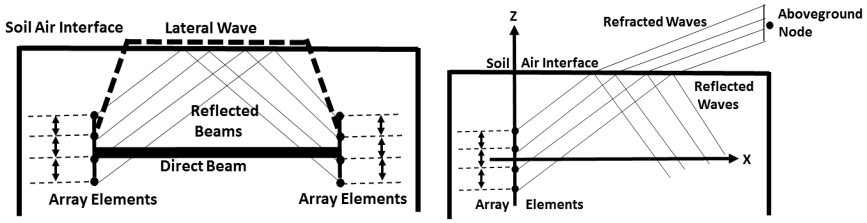

(a) (b)

Fig. 4.10: UG MIMO Communication [41]: (a) Receive Beamforming, (b) Transmit Beamforming

The capacity of three UG components of EM waves is given as:

$$C = \sum_{k=1}^{3} log_2(1 + SINR_k) \tag{4.26}$$

Main objective of the technique is to improve gain and reduce inter-component interference, therefore, only those beamforming vectors are considered which comes under the lower bound capacity. Next, the method to completely remove the inter-component interference will be presented. For every sensed wave component, instantaneous SNR can be calculated as:

$$\gamma_i = \frac{E_b \mid h_i \mid^2}{N_0}, \tag{4.27}$$

where i = Lateral direct and reflected components; $\mid h_i \mid$ is impulse response, and E_b is energy per bit. In contrast to single antenna match filter-based, SNR can be increased three times via maximum ratio combining (MRC) approach:

$$\gamma = \sum_{i=1}^{3} w_i \frac{E_b \mid h_i \mid^2}{N_0}, \tag{4.28}$$

where w_i is the combining weight. Although SISO achieves the maximum gain, however, interference due to reflected component is still present. Therefore, transmit beamforming vectors are used to suppress unwanted interference. Hence, received signal is represented as [7, 46]:

$$y_k = w_k^* TRf_k x_k + w_k^* I_k f_i x_i + w_k^* n_k \tag{4.29}$$

$$y_k = \frac{w_k^* TRf_k x_k}{||TRf_i||} + \frac{w_k^* I_k f_i x_i}{||TRf_i||} + \frac{w_k^* n_k}{||TRf_i||} \tag{4.30}$$

It is important for MRC approach to satisfy the following equation via transmit beamforming vector for complete removal of interference from equation 4.30

$$w_1^* I_1 f_i = 0 \tag{4.31}$$

UG MIMO adjusts the weights according to soil moisture, however, in addition to the environment-aware weight adjustment, it also uses the feedback mechanism. Feedback signals adjust the MIMO weights via array-gain feedback loops. The array gain is maximized using the pilot signals. UG MIMO array at transmitter adjust its parameter by receiving a pilot signal in receive mode. The transmitter channel state is determined by varying the scan angles while transmitter is operating in receive mode. Using the best statistics of SNR, parameters are adjusted with change in soil moisture.

Far-field power density for the identical element is calculated as follow [13, 43]:

$$P_{den} = \frac{\mid E(\theta,\phi) \mid^2}{120\pi}, \tag{4.32}$$

where $E(\theta,\phi)$ denotes the intensity of electric field for each individual array and is calculated as:

$$\mid E(\theta,\phi) \mid = \sqrt{P_{et}}\sqrt{G_{et}}\frac{\sqrt{30}}{d}, \tag{4.33}$$

where P_{et} is the transmit power, G_{et} is the transmit gain and d is the distance. Array gain G_a is calculated by getting sum of E-field contributions (E_a) from all elements [13, 38]. Therefore,

$$G_a(\theta,\phi) = \frac{d^2}{30}\frac{\mid E_a\zeta(\theta,\phi) \mid^2}{P_t}, \tag{4.34}$$

where ζ represents the element phase factor and

$$E_a = \frac{\sqrt{30}}{d}\sum_n \sqrt{P_{et}}\sqrt{G_{et}}. \tag{4.35}$$

E ective isotropic radiated power (EIRP) can be calculated as:

$$P_{rad} = G_t P_t, \tag{4.36}$$

where P_t is the power transmitted and G_t is the array gain. The far-field power density P_{av} is calculated as [8, 34]:

$$P_{av} = P_{av}^D + P_{av}^R + P_{av}^L. \tag{4.37}$$

where D is the power density of direct component, R is the power density of reflected component, and L is the power density of lateral component [147].

The received power is calculated by multiplying far-field power density P_{av} and antenna aperture $(\lambda_s^2/4\pi)$. The received power is expressed as [8, 42, 53]:

$$\begin{aligned}
P_r^d &= P_t + 20\log_{10}\lambda_s - 20\log_{10}r_1 - 8.69\alpha_s r_1 - 22 + 10\log_{10}D_{rl},\\
P_r^r &= P_t + 20\log_{10}\lambda_s - 20\log_{10}r_2 - 8.69\alpha_s r_2 - 20\log_{10}\Gamma - 22 + 10\log_{10}D_{rl},\\
P_r^L &= P_t + 20\log_{10}\lambda_s - 4\log_{10}d - 8.69\alpha_s(h_t + h_r) + 20\log_{10}T - 22 + 10\log_{10}D_{rl},
\end{aligned} \tag{4.38}$$

where Γ is the reflection coefficient, T is the transmission coefficient [8], and λ_s denotes wavelength in the soil. The received power of an isotropic antenna is calculated as [8]:

$$P_r = 10log_10\left(10^{\frac{p_r^d}{10}} + 10^{\frac{p_r^r}{10}} + 10^{\frac{p_r^L}{10}}\right). \tag{4.39}$$

4.5.2 Performance Analysis

This section analyze and evaluate the performance of UG MIMO model.

Transmit Beamforming: Transmit MMSE, MRT, and ZFBF beamforming technique in [5] are used for the evaluation. Heuristic beamforming techniques, such as ZFBF, MRT, transmit MMSE/regularized ZFBF/SLNR-MAX beamforming, and the corresponding power allocation, is also based on the [5, 65]. UG impulse response has been investigated with details in [52, 147]. Therefore, instead of generating a random OTA channel, UG impulse response presented in [147] is used for UG MIMO application. Fig. 4.11(b) shows a three-component model of the UG channel. SNR values are considered in range of $-10\,\mathrm{dB}$ to $30\,\mathrm{dB}$. For each approach, channel matrices are generated as a first step of simulation. From these channel matrices, a normalized beamforming matrices are calculated for each technique. UG MIMO is evaluated for all three components of UG channel and the sum rate is computed for all beamforming approaches.
Figs. 4.12 plots average sum rate with change in average SNR. Fig. 4.12(a), 4.12(b) and 4.12(c) shows average sum rate for one (direct), two (direct and reflected) and three (direct, lateral, and reflected) wave components, respectively. For single, there is no e ect of beamforming and all three approaches have same average sum rate of 1.5 to 1.7. In case of two components, the sum rate increased from 1.6 to 3.1 at average SNR of $10\,\mathrm{dB}$. All three approaches have minor di erence of 0.1 in average sum rate at SNR of $0\,\mathrm{dB}$. The di erence between ZFBF and MMSE increases with the increase in SNR, thus, MIMO UG shows better performance than ZFBF and have improved power gains which is further shown in Fig. 4.12(c). In case of two components, the sum rate increased from 3.1 to 6.6 at average SNR of $10\,\mathrm{dB}$ which increased to 8.4 at average SNR of $30\,\mathrm{dB}$. This high performance gain shows that UG MIMO performs to its maximum when all three components are used for transmit beamforming in underground environment

Receive Beamforming: To evaluate receive beamforming, a 16-element uniform linear array with an inter-element distance of half wavelength and $300\,\mathrm{MHz}$ of operational frequency is used. Path loss of UG communication increases with the frequency, therefore, lower range of frequency spectrum is used to achieve long-range communication. The three components of UG communication are shown in Fig. 4.11(a). The signal received at $10°$-$15°$ azimuth is the most powerful signal. The direct wave is received from $90°$ azimuth, and reflected signal reaches the receiver at $45°$ azimuth. Fig. 4.11(c) shows a spatial spectrum of receive beamforming for all components. The highest power gain is shown at $10°$ for lateral wave, second highest is at $90°$ for direct wave, and third highest is at $45°$ for reflected waves [51].

Impact of soil-air interface: The separation between soil and air medium is called soil-air interface. Both medium have di erent properties which causes waves refraction. This phenomenon is also termed as beam squint [18, 20]. Beam squint can cause an error of $5°$-$15°$, depending on soil moisture and incidence angle at interface. The velocity of wave is also a ected by refraction which is corrected

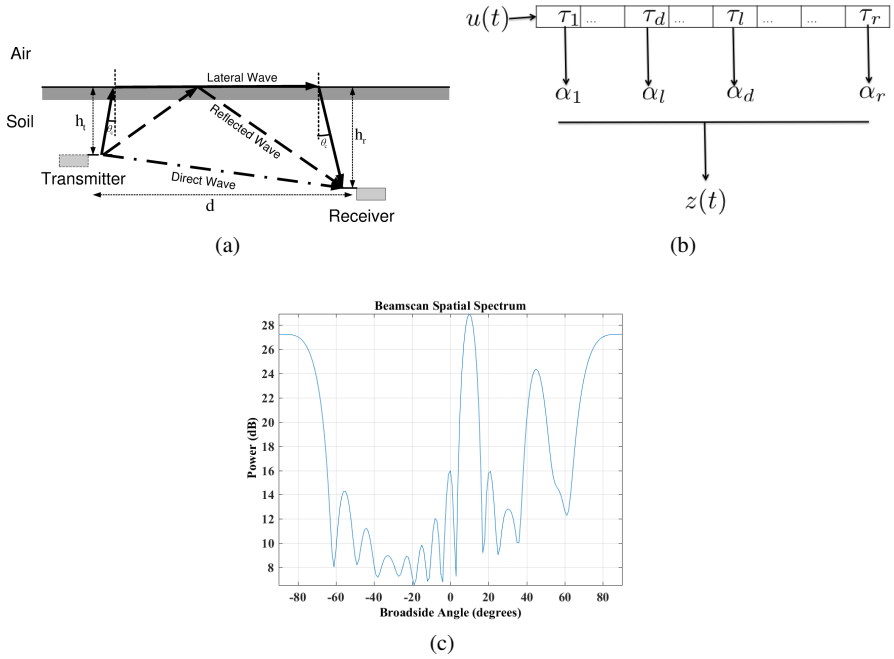

Fig. 4.11: (a) Three wave components in underground channel [147], (b) UG channel model realization with direct, lateral, and reflected components, (c) Spatial spectrum of the direct, lateral, and reflected components [41]

by angle adjustments and time delay (τ). Fig. 4.13(a) plots τ with change in soil moisture. It can be seen that τ increases with the increase in soil moisture and increasing depth further makes it worse. Fig. 4.13(b) shows the same plot but with adjustments made in original phase. It can be observed that phase has to be adjusted as per increase in soil moisture level and depth [24]. For each approach, channel matrices are generated as a first step of simulation. From these channel matrices, a normalized beamforming matrices are calculated for each technique. UG MIMO is evaluated for all three components of UG channel and the sum rate is computed for all beamforming approaches [47].

4.6 Cross-layer Modulation: On the use of Soil Properties

UG channel model shows that communication in WUSNs is e ected by various environmental parameters such as seasonal change, soil type, tunnel size, soil moisture variations, and antenna position/polarization. Therefore, it is important to design environment-adaptive protocols for WUSNs. Moreover, physical layer is

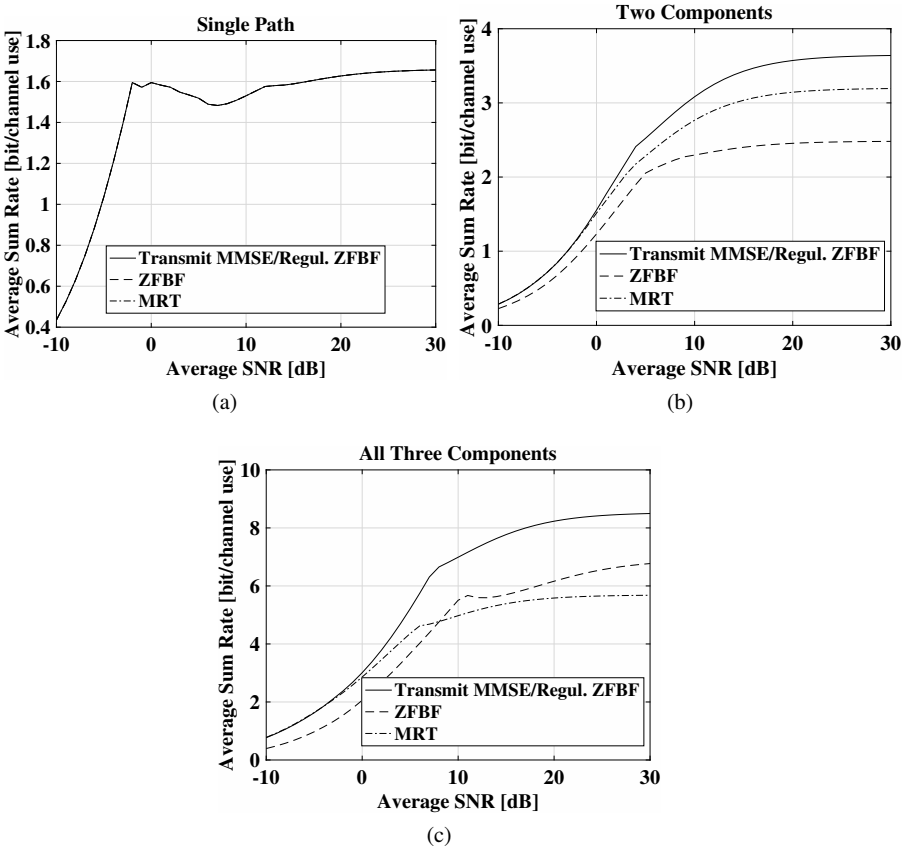

Fig. 4.12: Average sum rate v/s average SNR in UG MIMO [41]: (a) single-wave component path, (b) two-wave component paths, (c) three-wave component paths

quite unpredictable and directly e ect the quality of communication, therefore, for better performance, environment-adaptive cross layer protocols are required. To that end, a packet size optimization framework is presented for WUSNs [81]. The model will use the empirical results towards improving underground channel model by complete characterization of the UG channel. It will also identify the networking related challenges in the underground environment, e.g., e ects of soil on routing and medium access control. A simulation module for an underground communication will be given. This simulator will consist of rich and accurate models for underground communication. the purpose is to provide motivation for developing more accurate models for the UG communication.

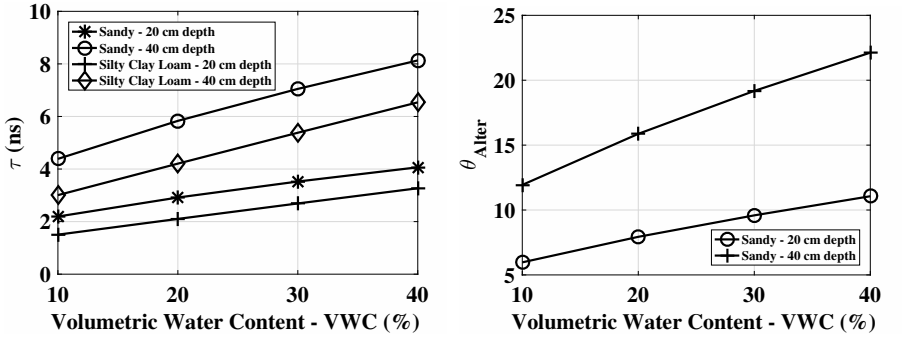

(a) (b)

Fig. 4.13: (a) Time Delay τ with change in soil moisture [41], (b) Phase shift adjustment with change in soil moisture [41]

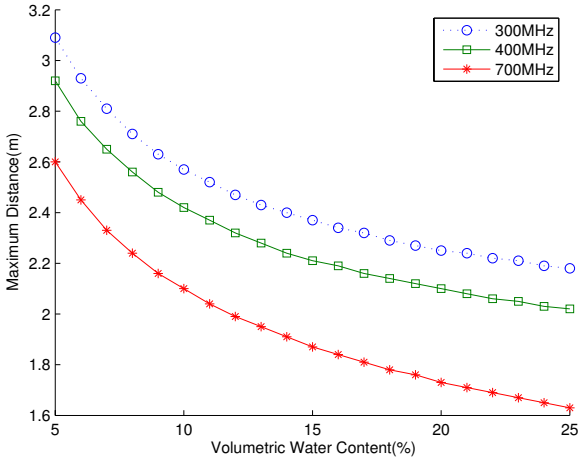

Fig. 4.14: Maximum inter-node distance with variation in volumetric water content (VWC)

4.6.1 Cross-layer Protocol Design

As discussed earlier, WUSN communication is e ected by dynamic environment parameters. Therefore, a cross-layer design should be able to adapt to those dynamically changing operating parameters to achieve efficient system performance. Fig. 4.14 shows that WUSN communication range is inversely proportional to the soil moisture. The achievable distance decreases with the increase in soil moisture

content. Although, the model gives a thorough idea of UG communication, however, its e ects on high-layer networking protocol are yet to be investigated.
There is a need of detailed empirical validation for the underground wireless channel. To that end, field experiments and software simulations are performed in a testbed setting. The testbed have 50 tested wireless sensor nodes. This testbed is used to develop a generic framework by evaluating following research issues:

4.6.1.1 Empirical Evaluations

In [27], authors have proposed an EM-based propagation model considering soil dielectric properties [28]. The model is empirically tested for signal strength of transmitting and receiving antenna, and packet loss rate in di erent testbeds (experiment sites). Results from these experiments are used to propose a more general channel model.

4.6.1.2 Medium Access Performance

Wireless communication medium is share by multiple nodes. In shared medium, a node can experience interference from neighboring nodes sharing the medium. Therefore, its is important to understand the di erence between the communication and interference by a node. For example, even if a node x is not able to communicate with some other node y, its communication with other nodes may still e ect the y communication as an interference. To that end, [33, 65] investigates the performance of multiple communicating sensors in presence of a controlled background traffic.

4.6.1.3 E ects of Seasonal Changes

Weather changes directly e ect the soil moisture and temperature, hence, causing the communication performance to change. To that end, seasonal e ects are evaluated for a period of 12-months to study the e ect of humidity, temperature, and precipitation on communication performance [27].

4.6.1.4 Development of a Cross-layer Communication Software Module

Empirical results will be used to develop, modify and improve the communication model to use the sensor information efficiently. The communication parameters such as signal strength, modulation scheme, route information and packet size, are determined using the real-time information from the sensor [30, 46].

4.6.2 Future Research Directions

WUSN paradigm can also be used for communication between underground and above-ground (AG) nodes, e.g., sinks, relay nodes or control units. The underground sensor node can send their data to some central location using AG nodes. Hence, WUSN provides the combination of UG and AG communication. To that end, communication characteristics of UG to AG communication can be further explored for research purposes, e.g., di erence in attenuation level of a signal in soil (UG) and air (AG). Investigation of this area can result in better understanding and further improvement of UG channel communication.

4.7 Medium Access in Wireless Underground Communications

Medium Access Control (MAC) is one of the important feature of wireless networks. Wireless Underground Sensor Networks (WUSN) architecture is distributed where each sensor attempts to communicate in a shared wireless channel [13]. Therefore, to implement an optimized and efficient WUSN, it is very important to improve the sharing mechanism by improving MAC protocols for WUSNs [11, 50]. These MAC protocols are analyzed by performing the underground-to-underground (UG2UG) communication experiments and simulations. The analysis shows that the behavior of communication parameters, e.g., interference and carrier ranges, is completely di erent for underground then what it is in over-the-air (OTA). This significant di erence results in increased contentions leading to large amount of packet collisions. A model is developed to capture the e ect of soil on the performance of medium access in an attempt to propose a novel MAC solution for underground sensor networks and eliminate possible shortcomings. Here, the MAC protocols for (WUSNs) are described [13, 49, 52]. This section discusses the performance of di erent traditional MAC protocols for underground environment, and study the feasibility of these MAC protocols for underground space and identify shortcomings due to complex communication medium [13].

4.7.0.1 Traditional Modulation Scheme

Modulation schemes such as Amplitude Shift Keying (ASK), Frequency Shift Keying (FSK) and Phase Shift Keying (PSK) are studied in [82] for their e ect on Bit Error Rate (BER) [1]. Fig. 4.15(a) shows the plot between VWC and maximum inter-node distance (with BER target of 10^{-3}) under various modulation schemes. It can be seen that PSK achieves the largest communication range, therefore, PSK is selected for the analysis [1].

4.7.0.2 Operation Frequency and Deployment Depth

In Fig.4.15(b), path loss is plotted against the burial depth H at di erent operating frequencies [1]. Path loss can be reduced by finding an optimal frequency at optimum depth. This is an important fact in WUSN as the sensor deployment in WUSNs is highly dependent upon the operating frequency of sensors [1]. Moreover, Fig.4.15(b) shows that path loss becomes tends to become constant as the depth increases. Hence, underground channel tends to become single-path channel with the increase in depth and negligible reflection. Therefore, two-path channel should be considered for lower depths [1].

4.8 Cost-E cient Underground Deployment

A cost-efficient deployment of sensor nodes is a challenge in WUSN paradigm and needs to be addressed. While deploying sensors in 3-dimensional environments, it is imperative to consider range and connectivity constraints. Communication range is also depends upon the depth of sensor nodes, hence, deployment depth should also be considered while analyzing the deployments strategies in WUSNs. Therefore, UG deployment [1, 25, 59, 81] becomes an optimization problem using minimum number of sensor nodes, with mentioned constraints, to achieve optimal performance and need novel optimization programming methods from networking paradigm. It is also important to consider the randomness of soil and weather conditions while deploying network of UG nodes. Deploying deterministic optimization technique to such random behaving network is a challenging task. Moreover, performance of base stations also su er from the e ect of soil-air interface, hence, a separate optimization model for base stations and an optimal routing protocol is also required for longer lifetime of the network. As sensor nodes are buried in underground at di erent depths, changing the battery of such sensors is also a challenging issue and needs to be addressed efficiently for longer life of network so that a certain level of performance can be guaranteed. Following research issues are discussed under UG deployments:

- *Deployment of sensors* - The network connectivity depends upon the connectivity of UG nodes between UG nodes and the sink nodes. The deployment of over-the-air wireless nodes has extensively been studied, however, UG development is yet to be explored. UG deployments is a NP-hard problem, therefore, heuristics are used to determine the optimal deployment strategies. Soil properties and e ect of environmental changes are additional factors to consider while deploying UG nodes. This is analyzed through sensitivity analysis for development of more robust deployment strategies [34, 43].
- *Deployment of the base stations* - In UG networks, base stations are located above-ground, therefore, attenuation of signal attenuation between two AG nodes is di erent from that of between AG and a UG node due to di erent communication medium. To that end, an optimization model is given for

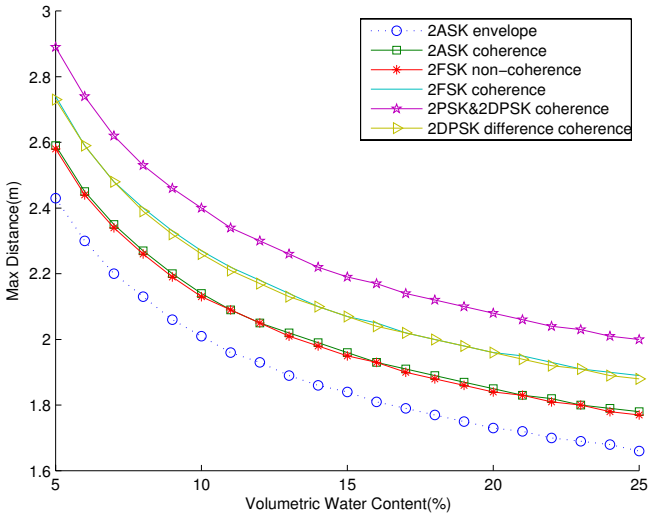

(a)

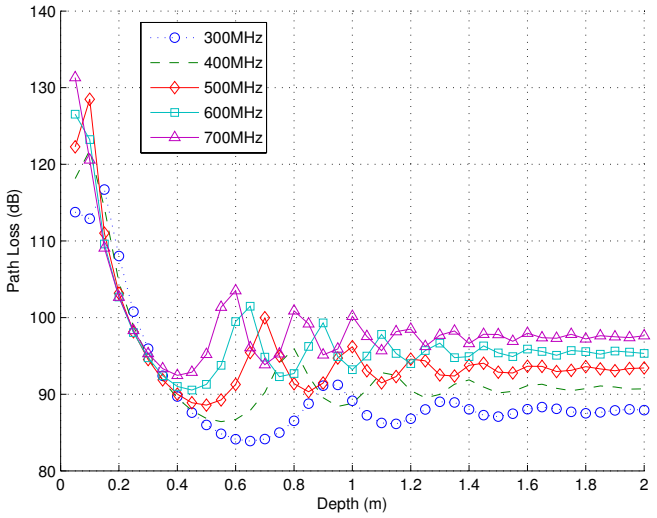

(b)

Fig. 4.15: (a) Maximum inter-node communication distance with variation in soil moisture [1], (b)Path loss with depth variations in two-path channel model [1]

determining the optimal number of base stations to deploy along-with their

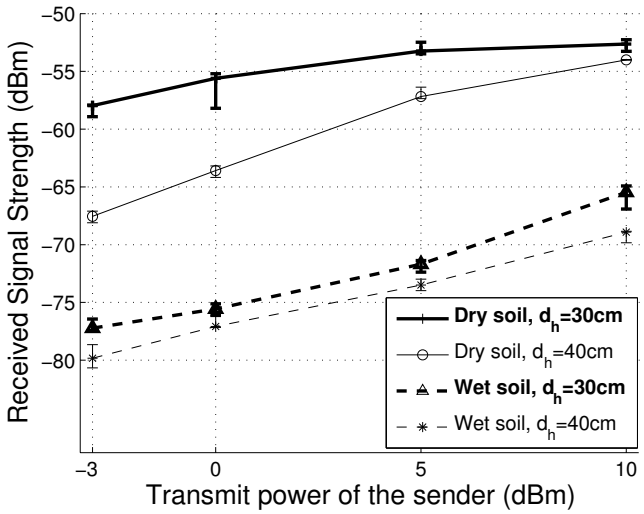

Fig. 4.16: RSS v/s transmitted power under various soil moisture levels [59]

optimal location. For multiple base station, deployment is modeled considering that they will communicate with each other [28, 36].

- *Routing policy* - Finally, after network deployment, an optimal routing protocol is determined. Randomness and uncertainty associated with the sensor lifetimes requires a simulation modeling to determine how long a network can last using a certain routing protocol. As all these parameters will be evaluated using a simulation, a sampling error may also occur in measurement. To that end, simulation optimization technique in [35, 53] will be used.

4.8.1 Simulation Results

To understand the e ect of soil properties on wireless communication and underground communication experiment is performed [59]. For this experiment, two sensors are used which are buried at 40cm. Experiment is performed using the separation distance, between both sensors, of 30cm and 40cm. Furthermore, to incorporate the e ect of environment, two types of soils are used for the experiment: dry soil and wet soil. The soils are taken from the location where 2.5% of precipitation was registered [86] giving the soil moisture of 11% for dry soil and 18% for wet soil. Fig. 4.16 plots the received power with the transmitted power for the experiment. It can be seen the received signal strength is 20 dB lower for the wet soil as compared to dry soil. It results in twice the communication error rate significantly e ecting the higher layer communication protocol.

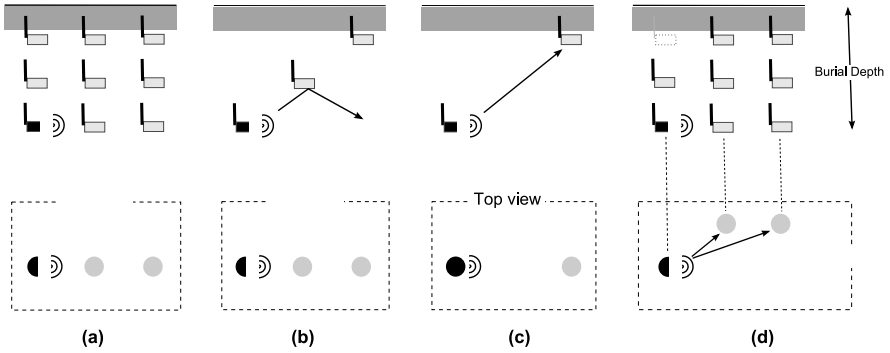

Fig. 4.17: The communication scenarios for underground transmitter and an aboveground transmitter [62]

Figs. 4.17 shows the communication scenarios for underground transmitter and an aboveground transmitter. The connectivity region of the UG transmitter consist of both UG and AG components, however, communciaiton range is very short due to high attenuation because of underground environment. On contrary, communication range of AG transmitter is relatively large as compared to that of UG node. AG range also consist of some *nulls* at the angles where UG signals get reflected. AG communication range in WUSN is similar to that of traditional over-the-air (OTA) wireless nodes. Short range of UG transmitter is mainly due to the fact that signals are highly reflected when enters from a medium of a lower density, i.e., air, to a medium of a higher density, i.e., soil [37, 42].

Most of the studies about network connectivity employ percolation theory, which was started by the pioneering work of Gilbert. The basic idea about percolation is that there is a critical density, λ_c, such that when the node density is greater than λ_c, there is a positive percolation probability that an arbitrary node belongs to a cluster of infinite size (supercritical phase); on the other hand, when the node density is smaller than λ_c, the percolation probability is zero (sub-critical phase) [47, 51].

Most of the literature, dealing with network connectivity utilize percolation theory, which will be the foundation of my research too. In [16, 20], the function of base station is similar to the above ground nodes in my WUSN consideration. According to the author, for the infinite 2-D plane, base station does not improve connectivity. However, in the WUSN field, it is finite, which I think will be more like the 2-D strip case, thus the deployment of the above ground nodes may help improve network connectivity.

The interference model in [15, 25, 27] shows if the connectivity of the network needs be kept with the impact of the interference, the orthogonality factor γ needs to be small. But, the conclusion is drawn under the assumption that the transmit power of each node is the same. According to [30, 45], designed transmit power assignment can be used to maintain network connectivity. The interference model in

[31] is simplified to consider interfering nodes individually, which is not true in real situation.

The unreliable link issue considered in [29, 65] is quite similar in WUSNs. However, the modeling of the dynamic as a Markov on-o process is not suitable for WUSNs, where the links are quite stable during short period but dramatically change caused by soil moisture. This process may be modeled as several di erent networks with di erent path loss function and transmit power. Thus, the connectivity of the network may be modeled as a set of several di erent networks.

4.8.2 E cient deployment for full connectivity of Ad-Hoc Networks

In this section, the possibility of deploying base stations to ensure connectivity when the node density, λ, is small, is considered. The results show that because of percolation there is no benefit in terms of connectivity in the supercritical phase and the benefit remains marginal in the sub-critical phase, unless the node spatial distribution is close to 1-dimensional [16, 50].

The transmission range of the nodes is modeled as a ball of radius $r/2$ and two nodes are neighbors if their representing balls intersect. Thus, the communication range is fixed at r. This model can be easily transformed to a graph [49].

The authors first consider the situation of a pure ad-hoc network for three di erence cases: 1-dimensional, 2-dimensional plane and 2-dimensional strip. For the 1-dimensional case, they calculate the connectivity probability, $P_c(x)$, of two nodes at distance x and find the bounds of the probability when $x \geq 2r$, which is

$$\begin{aligned} &(1-e^{\lambda r})e^{\lambda(x-2r)e^{-\lambda r}} - \lambda e^{-\lambda r} \\ \leq P_c(x) &\leq (1-e^{-\lambda r})e^{-\lambda(x-r)e^{-\lambda r}} \ . \end{aligned} \tag{4.40}$$

This leads to the conclusion that in one dimension, the network is almost surely (a.s.) divided into an infinite number of bounded clusters, between which no communication is possible [52, 72].

For the 2-dimensional case, the percolation theory holds such that there is a critical density λ_c for the supercritical phase and a unique unbound cluster a.s. The probability that an arbitrary node belongs to this unbound cluster is called percolation probability θ. We have $P_c(x) \geq \theta^2$ and $\inf_{x>0} P_c(x) = \theta^2$.

For the 2-dimensional trip with width d, percolation never occurs.

4.8.3 Topology Control Network Connectivity

The issue of topology control under the physical SINR model with the objective of maximizing network capacity is studied in this section. The intention of adopting the SINR model is that first the interference in the resulting topology is likely to be

high because the node degree does not capture interference adequately and second a wireless link that exists in the communication graph may in practice not exist under the physical model because of high interference[48].

In this section, a centralized approach (MaxSR) is proposed for topology control. This approach consists two parts: T2P and P2T. T2P optimizes the assignment of transmission power given a fixed topology to minimize the average interference degree, and P2T constructs, based on the power assignment, a new topology by deriving a spanning tree that gives the minimal interference degree [55, 71].

In their model, the communication graph is defined based on the received power at the receiver without consideration of interference. Thus, a link (v_i,v_j) is said to exist if and only if:

$$p_t(i) \geq \frac{d_{i,j}^{\alpha} RX_{min}}{g_{i,j}} \,, \tag{4.41}$$

where RX_{min} is the minimum received power requirement and $g_{i,j}$ is the path gain. Moreover, the interference is considered individually in the works [24, 54]. Interference node is defined such that the transmission of an interference node blocks the transmission on link (v_i,v_j). In other words, node k is an interference node for link (v_i,v_j) if

$$\frac{p_t(i) d_{i,j}^{-\alpha}}{N + p_t(k) d_{k,j}^{-\alpha}} < \beta \,. \tag{4.42}$$

The interference degree of a link (v_i,v_j) is defined as the number of interfering nodes for (v_i,v_j). The authors argue that interference degree is a better index than node degree in quantifying interference.

For *Topology to Power assignment*, and indicator function is employed to indicate if a link can transmit and the function is smoothened by the sigmoid function. The problem is then modeled as a linear programming problem. For *Power assignment to Topology*, interference degree is first calculated for each edge and exploited as the weight of the edge. Then, an algorithm similar to the minimum spanning treealgorithm is adopted to reconstruct the topology [32, 46]. Repeating those two algorithms alternately, the power assignment and the topology will converge to the optimal results.

4.9 Modeling the E ects of Interference

4.9.1 The Protocol Interference Model

Consider a pair of transmitter and receiver $\{X_i, X_{R(i)}\}$, where X_i and $X_{R(i)}$ denote a transmitting terminal and its corresponding receiving terminal, respectively. Communication over link $(X_i, X_{R(i)})$ is successful if the distance between the receiver $X_{R(i)}$ and any other terminal X_k transmitting on the same channel is larger than the distance between X_i and $X_{R(i)}$ by a factor $(1 + \Delta)$, that is

$$|X_k - X_{R(i)}| > (1+\Delta)|X_i - X_{R(i)}| \,. \tag{4.43}$$

4.9.2 The Physical Interference Model

Consider a pair of transmitter and receiver $\{X_i, X_{R(i)}\}$ with a transmit power assignment P_i, the transmission is successful if the signal to interference plus noise ration (SINR) at $X_{R(i)}$ is equal to or larger than a given threshold β, that is

$$\frac{\frac{P_i}{|X_i - X_{R(i)}|^\eta}}{N + \sum_{k \in V, k \neq i} \frac{P_k}{|X_k - X_{R(i)}|^\eta}} \geq \beta \,, \tag{4.44}$$

where N is the additive noise power.

4.10 Connectivity in Underground Environement

The fundamental property of a wireless network is to maintain connectivity between all network components (sensors and sinks) for proper functionality. However, connectivity definition for terrestrial wireless channel and underground wireless network are di erent. A terrestrial wireless network is considered *connected*, if a sensor node is connected to at-least one sink using multi-hop connection [17] Connectivity of a UG node can be defined in terms of either mobile or fixed AG sink nodes. A UG wireless sensor network is considered connected if a UG sensors is connected to at-least one *fixed* AG sink node, or at-least one *mobile* AG sink node once every maximum tolerable latency time t [78].

Connectivity analysis of a WUSN is much more complicated as compared to that of terrestrial wireless network. WUSN framework is complicated as it consist of two types of sensor nodes (UG and AG nodes), and three types of transmission links, i.e., underground-to-underground (UG2UG), underground-to-aboveground (UG2AG), and aboveground-to-underground (AG2UG) links [2, 7, 68]. Among three links, the transmission range of UG2UG is lowest due to soil [43, 77], transmission range of UG2AG is highest as most of the signal travels through air. AG2UG is lower that UG2AG because of reflection from soil-air interface [77]. Moreover, in WUSNs, there is a trade-o between connectivity and latency.

A WUSN system consists of multiple sensor nodes for sensing data, and sink nodes for collecting data from the sensor nodes. A sing sink node results in using large numbers of UG nodes (high density) are required to achieve full connectivity. However, high density of UG nodes increases the maintenance and deployment cost. Therefore, high density of UG nodes is not recommended, instead, number of AG nodes are increased [2, 7]. It is not recommended to deploy the AG nodes in field as it can e ect the everyday operation of application where they are deployed, e.g.,

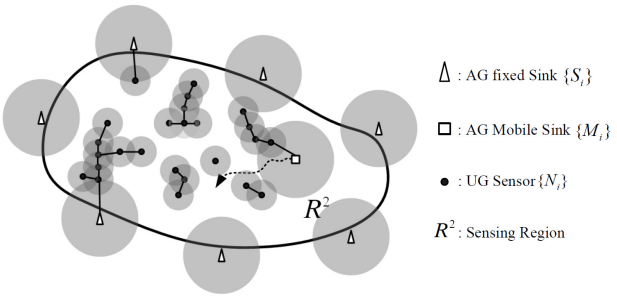

Fig. 4.18: WUSNs network topology [78] : Grey shaded region represents the range of each node for connecting with the other node

big machinery in agriculture cannot be used with high number of AG nodes. This constraint may cause the high density of sensor nodes on the border far from the field. To that end, AG nodes can be fixed on a mobile machinery and sensors far from field can send their data to sinks when machinery comes to their transmission range.

There has been already work done in analyzing the connectivity ad-hoc networks. For example, authors in [20], transmission ranges of nodes are scaled to get the connectivity, and in [3] maximum connectivity probability is computed using node density. Authors in [72] gives the simulation results to study the connectivity issues in mobile ad-hoc network. In [17], authors studies the connectivity in wireless network using single sink and [18] does it using multiple sinks. This section discusses the probability of connectivity in multi-hop wireless network using multiple sinks, environmental e ect on connectivity and latency-connectivity trade-o in wireless channel.

4.10.1 Channel Models

In [43], authors developed a WUSN channel model which is validated in [7, 77]. As discussed in previous section, WUSN channel model consist of three channels. The transmission of three channels are given below:

- *UG-UG Channel* - If power transmitted by the UG sensors is given by P_t^u, receiver and transmitter antenna gains are g_r and g_t, respectively. The received power is calculated as: $P_r^{U2U} = P_t^u + g_r + g_t - L_{UG-UG}$, where L_{UG-UG} is the path loss this channel. Similarly, the transmission range of UG-UG channel is given as [78]:

$$R_{UG-UG} = \max\{d : P_r^{U2U}/P_n > SNR_{th}\}, \tag{4.45}$$

where d is the distance is the distance between sending and transmitting sensor, noise is given as P_n, SNR_{th} represents minimum signal-to-noise ratio for receiver.

- *UG-AG Channel* - For a total received power of $P_r^{U-A} = P_t^u + g_r + g_t - L_{UG-AG}$, the transmission range for UG-AG channel is given as [78]:

$$R_{UG-AG} \simeq \max\{d_{AG} : P_r^{U-A}/P_n > SNR_{th}\} \tag{4.46}$$

- *AG-UG Channel* - Similarly, for a total received power of $P_r^{A-U} = P_t^a + g_r + g_t - L_{AG-UG}$, the transmission range for AG-UG channel is given as [78]:

$$R_{AG-UG} \simeq \max\{d : P_r^{A-U}/P_n > SNR_{th}\}. \tag{4.47}$$

Network Model

Fig.4.18 shows the network topology used for the analysis. The network consists of multiple UG sensor nodes and n fixed AG nodes and m mobile AG nodes, carried by some machinery, distributed in a WUSN region $\mathbb{R}^2$ where transmission range of nodes is much less than the region $\mathbb{R}^2$. There are two phases of communication: data from UG sensors is collected in sensing phase (using UG2UG channel) and data from sensing phase is reported to AG nodes in control phase (using UG2AG & AG2UG channel).

Mobility Model

Mobile AG nodes are fixed on equipment and field machinery. The mobility of machinery is modeled as random walk [13] and it's probability distribution function is given as follow:

$$P(t,(x_t,y_t)) = \frac{1}{2\pi t\sigma^2/\tau} \exp\left(- \frac{(x_t - x_0)^2 + (y_t - y_0)^2}{2t\sigma^2/\tau} \right) \tag{4.48}$$

where σ^2 is variance of the flight duration and τ is mean step time. A mobile AG sink will be more active when the value for σ^2 is larger and τ is smaller.

4.10.2 Lower & Upper Bound of the Connectivity Probability

Connectivity probability of a WUSN is dependent upon various dynamically changing environmental and system factors. Therefore, connectivity in WUSN can be given as a probability function. The lower bound on the probability function can be calculated from two quantities: (1) lower bound on a probability sensor deployed at location (x_i,y_i) connects with the sink at (x_j,y_i), $P(N_i^{(x_i,y_i)} \sim \text{Sink}_j^{(x_j,y_j)})$, in multi-hop

manner and first hit time of the random walk given in mobility model.The lower bound of connectivity probability is given as follow [78]:

$$P_c \geq \exp\{\lambda S_{fix} - \lambda S_{\mathbb{R}^2} + \lambda \int_{S_{\mathbb{R}^2 - S_{fix}}} [(1-F)\cdot G^m + 1 - G^m] dx_i dy_i\}. \tag{4.49}$$

where λ is the UG sensor node density, σ^2/τ is the mobility of mobile sinks, $S_{\mathbb{R}^2}$ is the area of region $\mathbb{R}^2$, S_{fix} is the area covered by fixed sink node in $\mathbb{R}^2$,

Similarly, upper bound on probability of not having an isolated UG node in WUSN is given as [78]:

$$P_c \leq \exp\{-\lambda \cdot e^{-\lambda \pi R^2_{UG2UG}} \cdot (S_{\mathbb{R}^2} - S_{fix}) \cdot H(m, R_{UG2AG}, \sigma^{-2}/\tau, t_s)\}. \tag{4.50}$$

where R_{UG2AG}, R_{UG2UG} are the transmission ranges, and t_s is the latency that can be tolerated during sensing phase.

4.10.3 Performance Evaluation

From equations 4.49 and 4.50, it can be observed the lower and upper connectivity probability bound of a WUSN is dependent upon various parameters. These bounds are validated by performing a simulation experiment in [78]. The simulation parameters are as follow: 12 fixed and 10 mobile AG nodes are deployed in 100m $\times$ 100 square grid. Fixed AG nodes follow uniform distribution and deployed at the border (3 at each corner), whereas mobile move as per random walk mode with $\sigma^2/\tau = 1m^2/s$. Tolerable latency in sensing and control phase are t_s =30s and t_c =20 min. Transmitting power is 10 mW, receiving and transmitting antenna gains are 5 dB, burial depth is kept 0.5 m and height of antenna at sink is 1 m. Soil moisture (VWC) is kept at 10%, sand particle 50%, and clay is 15%. Each simulation is run for 500 times and results are averaged. The bounds are calculated using equations 4.49 and 4.50. Fig. 4.19 and 4.20shows the simulation results to study the e ect of di erent parameters on connectivity.

1. *Soil Moisture* - Fig. 4.19(a) shows the connectivity probability with UG sensor density in wet (25% VWC) and dry soil (10% VWC). As the transmission range decreases in wet soil due to high water content, the UG nodes in wet soil scenario are doubled to get the equal connectivity probability. It can be seen that soil moisture significantly e ect the connectivity of WUSN and due to continuous dynamic change in soil moisture, connectivity status of WUSN also keeps in changing.
2. *Tolerable Latency* - Fig. 4.19(b) shows the connectivity probability with latency of the WUSN. With higher latency the connectivity of the WUSN increases. For

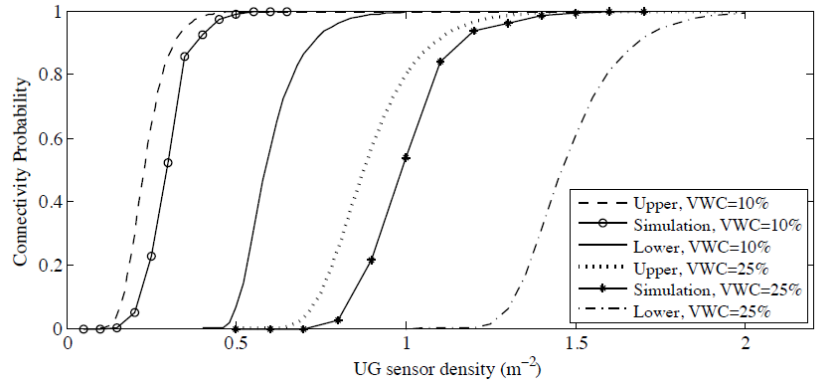

(a)

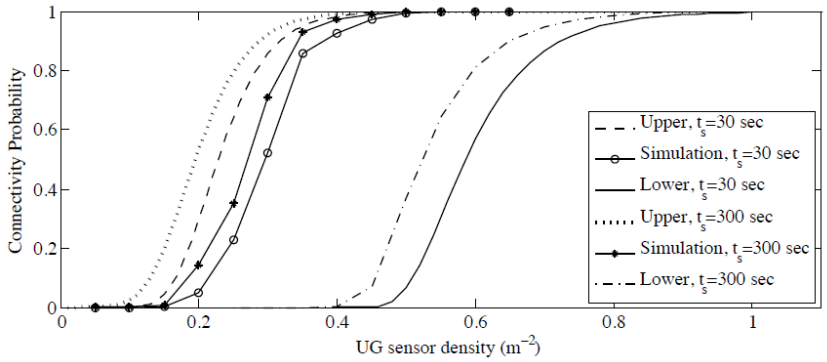

(b)

Fig. 4.19: Simulation Results [78]: (a) E ect of Soil Moisture, (b) Latency E ect

this simulation, the latency was increased from 30 to 300. Therefore, there is a trade-o between latency and WUSN connectivity.

3. *Depth and Height* - Fig. 4.20 shows the e ect of UG node depth and AG antenna height on connectivity probability of the WUSN. The depth of deployment significantly e ect the UG2AG and AG2UG communication whereas height e ects the AG2UG communication only. It can be seen in Fig.4.20(a), during sensing phase, that connectivity is significantly lower for depth over 2.5m. Conversely, connectivity probability increases with doubling the heoight in Fig. 4.20(b).

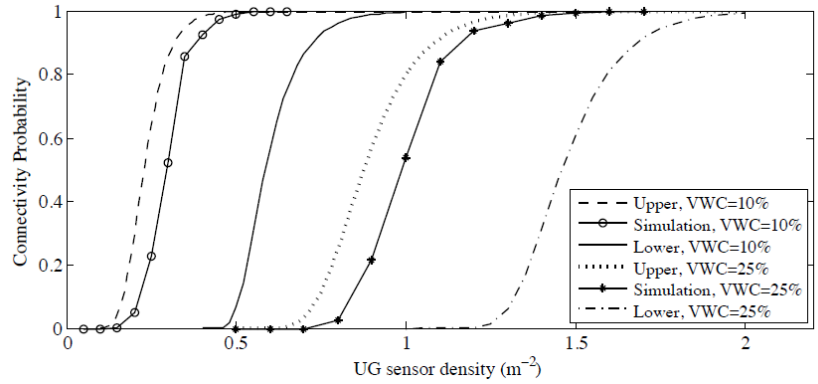

(a)

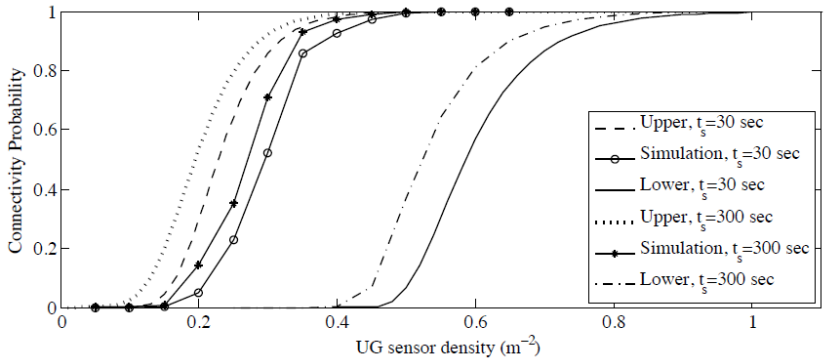

(b)

Fig. 4.20: Simulation Results [78]: (a) E ect of depth of UG node, (b) E ect of AG antenna height

References

[1] I. F. Akyildiz, Z. Sun, and M. C. Vuran. Signal propagation techniques for wireless underground communication networks. *Physical Communication Journal (Elsevier)*, 2(3):167–183, Sept. 2009.

[2] Ian F Akyildiz and Erich P Stuntebeck. Wireless underground sensor networks: Research challenges. *Ad Hoc Networks*, 4(6):669–686, 2006.

[3] Christian Bettstetter. On the minimum node degree and connectivity of a wireless multihop network. In *Proceedings of the 3rd ACM international symposium on Mobile ad hoc networking & computing*, pages 80–91, 2002.

[4] Trevor S Bird. Definition and misuse of return loss [report of the transactions editor-in-chief]. *IEEE Antennas and Propagation Magazine*, 51(2):166–167,

2009.

[5] Emil Björnson, Mats Bengtsson, and Björn Ottersten. Optimal multiuser transmit beamforming: A difficult problem with a simple solution structure [lecture notes]. *IEEE Signal Processing Magazine*, 31(4):142–148, 2014.

[6] HR Bogena, JA Huisman, H Meier, U Rosenbaum, and A Weuthen. Hybrid wireless underground sensor networks: Quantification of signal attenuation in soil. *Vadose Zone Journal*, 8(3):755–761, 2009.

[7] Chan-Byoung Chae, Insoo Hwang, Robert W Heath, and Vahid Tarokh. Interference aware-coordinated beamforming in a multi-cell system. *IEEE Transactions on Wireless Communications*, 11(10):3692–3703, 2012.

[8] Roger S Cheng and Sergio Verdú. Gaussian multiaccess channels with isi: Capacity region and multiuser water-filling. *IEEE Transactions on Information Theory*, 39(3):773–785, 1993.

[9] Peter S Chow and John M Cioffi. Bandwidth optimization for high speed data transmission over channels with severe intersymbol interference. In *[Conference Record] GLOBECOM'92-Communications for Global Users: IEEE*, pages 59–63. IEEE, 1992.

[10] Thomas M Cover and Joy A Thomas. *Elements of information theory*. John Wiley & Sons, 2012.

[11] I. Demirkol, C. Ersoy, and F. Alagöz. MAC protocols for wireless sensor networks: A survey. *IEEE Communications Magazine*, 44(4):115–121, 2006.

[12] Xin Dong and Mehmet C Vuran. A channel model for wireless underground sensor networks using lateral waves. In *2011 IEEE Global Telecommunications Conference-GLOBECOM 2011*, pages 1–6. IEEE, 2011.

[13] Xin Dong and Mehmet C Vuran. Empirical analysis of the hidden terminal problem in wireless underground sensor networks. In *International Conference on Wireless Communications in Unusual and Confined Areas (ICWCUCA)*, Aug. 2012.

[14] Xin Dong and Mehmet C Vuran. Impacts of soil moisture on cognitive radio underground networks. In *2013 First International Black Sea Conference on Communications and Networking (BlackSeaCom)*, pages 222–227. IEEE, 2013.

[15] O. Dousse, F. Baccelli, and P. Thiran. Impact of interferences on connectivity in ad hoc networks. *IEEE/ACM Transactions on Networking*, 13(2):425 – 436, April 2005.

[16] O. Dousse, P. Thiran, and M. Hasler. Connectivity in ad-hoc and hybrid networks. In *Proc. INFOCOM 2002*, volume 2, pages 1079–1088, New York, Jun. 2002.

[17] Olivier Dousse, Petteri Mannersalo, and Patrick Thiran. Latency of wireless sensor networks with uncoordinated power saving mechanisms. In *Proceedings of the 5th ACM international symposium on Mobile ad hoc networking and computing*, pages 109–120, 2004.

[18] Flavio Fabbri and Roberto Verdone. A statistical model for the connectivity of nodes in a multi-sink wireless sensor network over a bounded region. In *2008 14th European Wireless Conference*, pages 1–6. IEEE, 2008.

[19] A.J. Fenn and P.T. Hurst. *Ultrawideband Phased Array Antenna Technology for Sensing and Communications Systems*. MIT Press, 2015.

[20] Piyush Gupta and Panganamala R Kumar. Critical power for asymptotic connectivity in wireless networks. In *Stochastic analysis, control, optimization and applications*, pages 547–566. Springer, 1999.

[21] R.L. Haupt. *Timed Arrays*. Wiley, 2015.

[22] Irving Kalet. The multitone channel. *IEEE transactions on communications*, 37(2):119–124, 1989.

[23] A.K. Khandani. Media-based modulation: Converting static rayleigh fading to awgn. In *In 2014 IEEE International Symposium on Information Theory (ISIT)*, pages 1549–1553, June 2014.

[24] Abhiteja Konda, Advaith Rau, Michael A. Stoller, Jay M. Taylor, Abdul Salam, Gabriel A. Pribil, Christos Argyropoulos, and Stephen A. Morin. Soft microreactors for the deposition of conductive metallic traces on planar, embossed, and curved surfaces. *Advanced Functional Materials*, 28(40):1803020, 2018.

[25] L. Li, M. C. Vuran, and I. F. Akyildiz. Characteristics of underground channel for wireless underground sensor networks. In *Proc. Med-Hoc-Net 07*, Corfu, Greece, June 2007.

[26] Li Li, Mehmet C Vuran, and Ian F Akyildiz. Characteristics of underground channel for wireless underground sensor networks. In *Proc. Med-Hoc-Net*, volume 7, pages 13–15, 2007.

[27] Rui Ma and Wei Zhang. Adaptive mqam for energy harvesting wireless communications with 1-bit channel feedback. *IEEE Transactions on Wireless Communications*, 14(11):6459–6470, 2015.

[28] N. Peplinski, F. Ulaby, and M. Dobson. Dielectric properties of soils in the 0.3-1.3-ghz range. *IEEE Trans. Geoscience and Remote Sensing*, 33(3):803–807, May 1995.

[29] John G Proakis and Masoud Salehi. *Digital communications*, volume 4. McGraw-hill New York, 2001.

[30] GNU Radio. Gnu radio website.

[31] Ettus Research. Ettus research website.

[32] Wonjong Rhee and John M Cioffi. Increase in capacity of multiuser ofdm system using dynamic subchannel allocation. In *VTC2000-Spring. 2000 IEEE 51st Vehicular Technology Conference Proceedings (Cat. No. 00CH37026)*, volume 2, pages 1085–1089. IEEE, 2000.

[33] A. Salam and Mehmet C. Vuran. Impacts of soil type and moisture on the capacity of multi-carrier modulation in internet of underground things. In *Proc. of the 25th ICCCN 2016*, Waikoloa, Hawaii, USA, Aug 2016.

[34] A. Salam and Mehmet C. Vuran. Em-based wireless underground sensor networks. pages 247–285, 2017.

[35] Abdul Salam. Pulses in the sand: Long range and high data rate communication techniques for next generation wireless underground networks. *ETD collection for University of Nebraska - Lincoln*, (AAI10826112), 2018.

[36] Abdul Salam. A comparison of path loss variations in soil using planar and dipole antennas. In *2019 IEEE International Symposium on Antennas and Propagation*. IEEE, Jul 2019.

[37] Abdul Salam. Design of subsurface phased array antennas for digital agriculture applications. In *Proc. 2019 IEEE International Symposium on Phased Array Systems and Technology (IEEE Array 2019)*, Waltham, MA, USA, October 2019.

[38] Abdul Salam. A path loss model for through the soil wireless communications in digital agriculture. In *2019 IEEE International Symposium on Antennas and Propagation*, pages 1–2. IEEE, Jul 2019.

[39] Abdul Salam. Sensor-free underground soil sensing. In *ASA, CSSA and SSSA International Annual Meetings (2019)*. ASA-CSSA-SSSA, 2019.

[40] Abdul Salam. Subsurface mimo: A beamforming design in internet of underground things for digital agriculture applications. *Journal of Sensor and Actuator Networks*, 8(3), 2019.

[41] Abdul Salam. Subsurface mimo: A beamforming design in internet of underground things for digital agriculture applications. *Journal of Sensor and Actuator Networks*, 8(3):41, 2019.

[42] Abdul Salam. *Underground Environment Aware MIMO Design Using Transmit and Receive Beamforming in Internet of Underground Things*, pages 1–15. Springer International Publishing, Cham, 2019.

[43] Abdul Salam. An underground radio wave propagation prediction model for digital agriculture. *Information*, 10(4), 2019.

[44] Abdul Salam. An underground radio wave propagation prediction model for digital agriculture. *Information*, 10(4):147, 2019.

[45] Abdul Salam. Underground soil sensing using subsurface radio wave propagation. In *5th Global Workshop on Proximal Soil Sensing*, Columbia, MO, May 2019.

[46] Abdul Salam. *Internet of Things for Environmental Sustainability and Climate Change*, pages 33–69. Springer International Publishing, Cham, 2020.

[47] Abdul Salam. *Internet of Things for Sustainability: Perspectives in Privacy, Cybersecurity, and Future Trends*, pages 299–327. Springer International Publishing, Cham, 2020.

[48] Abdul Salam. *Internet of Things for Sustainable Community Development*. Springer Nature, 1 edition, 2020.

[49] Abdul Salam. *Internet of Things for Sustainable Community Development: Introduction and Overview*, pages 1–31. Springer International Publishing, Cham, 2020.

[50] Abdul Salam. *Internet of Things for Sustainable Forestry*, pages 147–181. Springer International Publishing, Cham, 2020.

[51] Abdul Salam. *Internet of Things for Sustainable Human Health*, pages 217–242. Springer International Publishing, Cham, 2020.

[52] Abdul Salam. *Internet of Things for Sustainable Mining*, pages 243–271. Springer International Publishing, Cham, 2020.

[53] Abdul Salam. *Internet of Things for Water Sustainability*, pages 113–145. Springer International Publishing, Cham, 2020.

[54] Abdul Salam. *Internet of Things in Agricultural Innovation and Security*, pages 71–112. Springer International Publishing, Cham, 2020.

[55] Abdul Salam. *Internet of Things in Sustainable Energy Systems*, pages 183–216. Springer International Publishing, Cham, 2020.

[56] Abdul Salam. *Internet of Things in Water Management and Treatment*, pages 273–298. Springer International Publishing, Cham, 2020.

[57] Abdul Salam. Wireless underground communications in sewer and stormwater overflow monitoring: Radio waves through soil and asphalt medium. *Information*, 11(2), 2020.

[58] Abdul Salam, Anh Duy Hoang, Atluri Meghna, Dylan R Martin, Gabriel Guzman, Yung Han Yoon, Jacob Carlson, Jordan Kramer, Keim Yansi, Michael Kelly, et al. The future of emerging iot paradigms: Architectures and technologies. 2019.

[59] Abdul Salam and Umit Karabiyik. A cooperative overlay approach at the physical layer of cognitive radio for digital agriculture. In *Third International Balkan Conference on Communications and Networking 2019 (BalkanCom'19)*, Skopje, Macedonia, the former Yugoslav Republic of, June 2019.

[60] Abdul Salam and Umit Karabiyik. A cooperative overlay approach at the physical layer of cognitive radio for digital agriculture. 2019.

[61] Abdul Salam and Syed Shah. Internet of things in smart agriculture: Enabling technologies. In *2019 IEEE 5th World Forum on Internet of Things (WF-IoT)*, pages 692–695. IEEE, 2019.

[62] Abdul Salam and Mehmet C Vuran. Impacts of soil type and moisture on the capacity of multi-carrier modulation in internet of underground things. In *2016 25th International Conference on Computer Communication and Networks (ICCCN)*, pages 1–9. IEEE, 2016.

[63] Abdul Salam and Mehmet C Vuran. Smart underground antenna arrays: A soil moisture adaptive beamforming approach. In *IEEE INFOCOM 2017-IEEE Conference on Computer Communications*, pages 1–9. IEEE, 2017.

[64] Abdul Salam and Mehmet C Vuran. Wireless underground channel diversity reception with multiple antennas for internet of underground things. In *2017 IEEE International Conference on Communications (ICC)*, pages 1–7. IEEE, 2017.

[65] Abdul Salam, Mehmet C Vuran, Xin Dong, Christos Argyropoulos, and Suat Irmak. A theoretical model of underground dipole antennas for communications in internet of underground things. *IEEE Transactions on Antennas and Propagation*, 2019.

[66] Abdul Salam, Mehmet C Vuran, and Suat Irmak. Pulses in the sand: Impulse response analysis of wireless underground channel. In *IEEE INFOCOM 2016-The 35th Annual IEEE International Conference on Computer Communications*, pages 1–9. IEEE, 2016.

[67] Abdul Salam, Mehmet C. Vuran, and Suat Irmak. Di-sense: In situ real-time permittivity estimation and soil moisture sensing using wireless underground communications. *Computer Networks*, 151:31 – 41, 2019.

[68] Abdul Salam and Mehmet Can Vuran. Smart underground antenna arrays: A soil moisture adaptive beamforming approach. In *Proc. IEEE INFOCOM 2017*, Atlanta, USA, May 2017.

[69] Abdul Salam and Mehmet Can Vuran. Wireless underground channel diversity reception with multiple antennas for internet of underground things. In *Proc. IEEE ICC 2017*, Paris, France, May 2017.

[70] Abdul Salam, Mehmet Can Vuran, and Suat Irmak. Pulses in the sand: Impulse response analysis of wireless underground channel. In *The 35th Annual IEEE International Conference on Computer Communications (INFOCOM 2016)*, San Francisco, USA, April 2016.

[71] Abdul Salam, Mehmet Can Vuran, and Suat Irmak. Towards internet of underground things in smart lighting: A statistical model of wireless underground channel. In *Proc. 14th IEEE International Conference on Networking, Sensing and Control (IEEE ICNSC)*, Calabria, Italy, May 2017.

[72] Paolo Santi and Douglas M. Blough. The critical transmitting range for connectivity in sparse wireless ad hoc networks. *IEEE transactions on Mobile Computing*, 2(1):25–39, 2003.

[73] Ehsan Seifi, Mehran Atamanesh, and Amir K. Khandani. Media-based MIMO: A new frontier in wireless communications. *CoRR*, abs/1507.07516, 2015.

[74] A. R. Silva and M. C. Vuran. Empirical evaluation of wireless underground-to-underground communication in wireless underground sensor networks. In *Proc. IEEE DCOSS '09*, Marina Del Rey, CA, June 2009.

[75] A. R. Silva and M. C. Vuran. Development of a Testbed for Wireless Underground Sensor Networks. *EURASIP Journal on Wireless Communications and Networking*, 2010, 2010.

[76] A. R. Silva and M. C. Vuran. Development of a Testbed for Wireless Underground Sensor Networks. *EURASIP Journal on Wireless Communications and Networking*, 2010.

[77] Agnelo R Silva and Mehmet C Vuran. Development of a testbed for wireless underground sensor networks. *EURASIP Journal on Wireless Communications and Networking*, 2010:1–14, 2010.

[78] Zhi Sun and I.F. Akyildiz. Connectivity in wireless underground sensor networks. In *Proc. of IEEE Communications Society Conference on Sensor Mesh and Ad Hoc Communications and Networks (SECON '10)*, Boston, MA, 2010.

[79] Samil Temel, Mehmet C Vuran, Mohammad MR Lunar, Zhongyuan Zhao, Abdul Salam, Ronald K Faller, and Cody Stolle. Vehicle-to-barrier communication during real-world vehicle crash tests. *Computer Communications*, 127:172–186, 2018.

[80] M. J. Tiusanen. Wireless Soil Scout prototype radio signal reception compared to the attenuation model. *Precision Agriculture*, 10(5):372–381, November 2008.

[81] M. C. Vuran and I. F. Akyildiz. Packet size optimization for wireless terrestrial, underwater, and underground sensor networks. In *Proc. IEEE INFOCOM '08*, Phoeniz, AZ, April 2008.

[82] M.C. Vuran and I.F. Akyildiz. Cross-layer packet size optimization for wireless terrestrial, underwater, and underground sensor networks. In *INFOCOM 2008. The 27th Conference on Computer Communications. IEEE*, pages 226 –230, 2008.

[83] Mehmet C. Vuran, Abdul Salam, Rigoberto Wong, and Suat Irmak. Internet of underground things in precision agriculture: Architecture and technology aspects. *Ad Hoc Networks*, 2018.

[84] Mehmet Can Vuran, Abdul Salam, Rigoberto Wong, and Suat Irmak. Internet of underground things: Sensing and communications on the field for precision agriculture. In *2018 IEEE 4th World Forum on Internet of Things (WF-IoT) (WF-IoT 2018)*, , Singapore, February 2018.

[85] Ariton E Xhafa, Ozan K Tonguz, Ahmet G Cepni, Daniel D Stancil, Pavel V Nikitin, and Dagfin Brodtkorb. On the capacity limits of hvac duct channel for high-speed internet access. *IEEE transactions on communications*, 53(2):335–342, 2005.

[86] Noaa's national weather service weather forecast office. http://www.crh.noaa.gov/gid/?n=neb_rainfall_observed#archive.

[87] SoilNet - A Zigbee Based Soil Moisture Sensor Network. http://www.fz-juelich.de/icg/icg-4/index.php?index=739. Project Group - Institute Of Chemistry And Dynamics Of The Geosphere (ICG) - Agrosphere Institute - ICG 4.